Localised upheaval buckling of buried subsea pipelines

Zhenkui Wang[a], G.H.M. van der Heijden[b,*], Yougang Tang[a]

[a] State Key Laboratory of Hydraulic Engineering Simulation and Safety, Tianjin University, Tianjin 300072, China

[b] Department of Civil, Environmental and Geomatic Engineering, University College London, London WC1E 6BT, UK

Corresponding author: G.H.M. van der Heijden, g.heijden@ucl.ac.uk

Abstract: Buried subsea pipelines under high temperature conditions tend to relieve their axial compressive force by forming localised upheaval buckles. This phenomenon is traditionally studied as a kind of imperfect column buckling problem. We study upheaval buckling as a genuinely localised buckling phenomenon without making any ad hoc assumptions on the shape of the buckled pipeline. We combine this buckling analysis with a detailed state-of-the-art nonlinear pipe-soil interaction model that accounts for the effect of uplift peak soil resistance for buried pipelines. This allows us to investigate the effect of cover depth of subsea pipelines on their load-deflection behaviour. Furthermore, the influence of axial and uplift peak soil resistance on the localised upheaval behaviour is investigated and the maximum axial compressive stress during the buckling process is discussed. Parameter studies reveal a limit to the temperature difference for safe operation of the pipeline. Localised upheaval buckling may then occur if the pipe is sufficiently imperfect or sufficiently dynamically perturbed.

Keywords: Buried subsea pipelines; Localised upheaval buckling; nonlinear pipe-soil interaction model.

1. Introduction

Subsea pipelines are increasingly being required to operate at higher temperatures. A buried pipeline exposed to compressive effective axial forces induced by high temperature and high pressure may get unstable and move vertically out of the seabed if the cover has insufficient resistance. This may be acceptable if the pipe integrity can be maintained in the post-buckled condition. But no guidance on pipe integrity checks in the post-buckled condition is provided in existing design codes. So the design procedure should ensure that the pipeline remains in place with a given tolerance for failure [1]. A pipeline buried in a trench is sufficiently confined in the lateral direction by the passive resistance of the trench walls. Restraint in the vertical direction is provided by the backfilled soil, whose minimum required depth is a key design parameter for pipeline engineers [2]. Under-designed cover depth may promote upward movement in the pipeline. In extreme cases, the pipeline may protrude through the soil cover, a phenomenon known as upheaval buckling. Upheaval buckling can have severe consequences for the integrity of a pipeline, such as excessive plastic deformation. Consequently, some engineering measures have been taken to prevent the upheaval buckling of subsea pipelines, such as burying and rock-dumping, or relieving the stress with in-line expansion spools [3, 4]. The uplift soil resistance of a buried pipeline is nonlinear during the process of upheaval buckling [5-7]. The uplift soil resistance reaches a peak value at a small uplift displacement, then decreases from this peak value to the pipe weight gradually due to the decreasing buried depth. The uplift peak soil resistance depends on the cover depth. Thus, it is necessary to study the influence of nonlinear uplift soil resistance and cover depth of the pipeline on localised upheaval buckling.

Much of the past work on pipeline buckling is based on Hobbs's work [8, 9], which itself is based on the very similar work on the buckling of railway tracks. In this work the whole pipeline is divided into three separate zones, a central buckled region and two adjoining straight regions. Based on this approach, Taylor derived an analytical solution to lateral and upheaval buckling for pipelines with initial imperfection [10-12] and analytical solutions for ideal submarine pipelines by considering a deformation-dependent resistance force model [13, 14]. A consistent theory is also developed for the analysis of upheaval buckling for imperfect heated pipelines by Pedersen and Jensen [15]. A similar column buckling approach (using slightly different boundary conditions) was used by Croll to study upheaval buckling of pipelines with geometrical imperfections [16]. Hunt took a standard formulation for upheaval buckling to study the effects of asymmetric bed imperfections, typified by a step, rather than symmetric imperfections such as a prop of infiltrated material between the pipe and the bed [17]. Moreover, small-scale model tests were conducted to understand the mechanism of upheaval buckling of buried pipelines [18, 19].

More recently, Hobbs's method has been adopted by several other studies. Wang and Shi [20, 21] investigated the upheaval buckling for ideal straight pipelines and for pipelines with prop imperfection on a plastic soft seabed. Also, analytical solutions were proposed and compared with finite-element simulations for high-order buckling modes of ideal pipelines and subsea

pipelines with a single-arch initial imperfection [22, 23], which were all based on the classical lateral buckling modes proposed by Hobbs. Karampour and co-workers investigated the interaction between upheaval or lateral buckling and propagation buckling of subsea pipelines [24-26]. Wang et al. investigated controlled lateral buckling [27] and the influence of a distributed buoyancy section on the lateral buckling [28] for unburied subsea pipelines using an analytical method. There were two limitations in these researches. First, these studies were all based on the assumption of one buckled region and two adjoining regions for the whole pipeline. Several boundary conditions were introduced when this assumption was employed, which may constrain the lateral or vertical deformation of the pipeline. Second, the lateral or vertical soil resistance was assumed constant to simplify the theoretical results.

In addition, many finite-element analyses have been performed to investigate upheaval buckling. Upheaval buckling of unburied subsea pipelines and pipe-in-pipe systems was studied by Wang et al. through finite-element modelling [29, 30]. Finite-element modelling was employed to investigate the critical upheaval buckling force of buried subsea pipelines [31-33] and post-buckling beahviour of unburied subsea pipelines and pipe-in-pipe systems [29, 30]. The nonlinear soil resistance model is proposed based on laboratory tests, which is also incorporated in finite element analysis of buried pipelines with different amplitudes of initial geometric imperfections [34]. Using genetic programming, Nazari et al. investigated the effect of uncertainty in soil, operating condition and pipe properties on upheaval buckling behaviour of offshore pipeline buried in clayey soil through a two-dimensional finite-element model [35]. An upheaval buckling solution to mitigate upheaval buckling risk was proposed using a preheating method combined with constraints from two segmented ditching constructions by Zhao and Feng and validated by a finite-element model [36].

For the central buckled region Hobbs takes a sine wave and introduces decay by means of imperfections. It is good to point out, however, that for this type of beam-on-foundation problems there exists a mechanism for genuine localised buckling that does not require one to make such ad hoc approximations. In this paper we discuss this localised buckling in some detail, show how localised solutions can be conveniently and reliably computed and compare results with those of Hobbs. We also use a realistic soil resistance model, which leads to differences in the load-deflection curves.

Localised buckling is quite different from (Euler) column buckling. It is described by a so-called Hamiltonian-Hopf bifurcation rather than the pitchfork bifurcation of column buckling. An important consequence is that unlike the critical load for column buckling, which depends strongly (quadratically) on the length of the structure, the critical load for localised buckling does not depend on this length (although the structure of course has to be long enough to support a localised buckle). Importantly, the critical load for localised buckling is found to be lower than that for Euler buckling. Although this critical load is generally not reached and localised deflection is initiated by imperfections or perturbations, this critical load still provides a useful reference load. For sufficiently long slender structures, localised buckling is also energetically much more favourable than periodic buckling into a (large) number of half sine waves [37].

The advantage of describing localised buckling by means of branches of solutions emanating from a Hamiltonian-Hopf bifurcation is that these solutions come with simple analytical estimates (in terms of the linear system parameters) for the 'wavelength' of the buckling pattern (e.g., the length of pipe in the central buckle) as well as the decay rate of successive buckles, without the need for some kind of damping or imperfections.

Of the few papers on pipeline buckling that do not make Hobbs's assumption of separate buckled and adjoining regions we mention the work of Zhu et al. [38] and Wang and van der Heijden [39] both of which studied localised lateral buckling of straight pipelines by analytical methods without making an assumed-mode approximation. Localised lateral buckling of partially embedded subsea pipelines with nonlinear soil resistance was also studied by Zeng and Duan [40]. In the present paper we consider localised upheaval buckling rather than lateral buckling.

As to the soil modelling, constant vertical soil resistance was incorporated into the upheaval buckling problem. Wang et al. [41] presented a perturbation analysis for upheaval buckling of imperfect buried pipelines based on nonlinear pipe-soil interaction, which however was only applicable to small vertical displacement. In this paper, a new nonlinear vertical soil resistance model is proposed, which can be applied to large vertical movement and is described in detail in the following section.

The purpose of this paper is therefore twofold. (i) We show that thermal pipeline buckling is well described by genuinely localised (and exponentially decaying) solutions that bifurcate from the straight pipe at a critical temperature. We explore the consequences of this localised buckling phenomenon without making any additional assumptions and pick up a few simple analytical results that may be useful as design formulas. (ii) We employ a realistic state-of-the-art nonlinear pipe-soil interaction model to compute load-deflection curves that take into account uplift peak resistance for buried pipelines.

The rest of the paper is organised as follows. In Section 2 we present the mathematical modelling of upheaval pipeline buckling, with the soil resistance model discussed in detail in Section 2.3. The method for computing localised solutions is explained in Section 2.4. It uses a shooting method and symmetry properties of the equilibrium equation. Parameter studies are carried out by numerical continuation (path following) techniques in Section 3. We also compare our solutions with those of Hobbs. Furthermore, the influence of the nonlinear vertical soil resistance model and cover depth on localised upheaval buckling is studied and discussed. Section 4 closes this study with some conclusions.
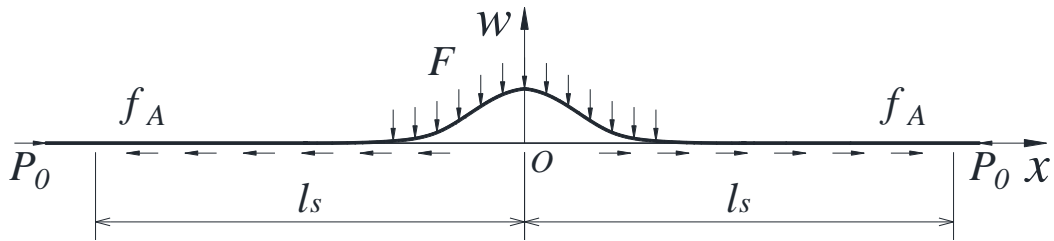
2. Problem modelling

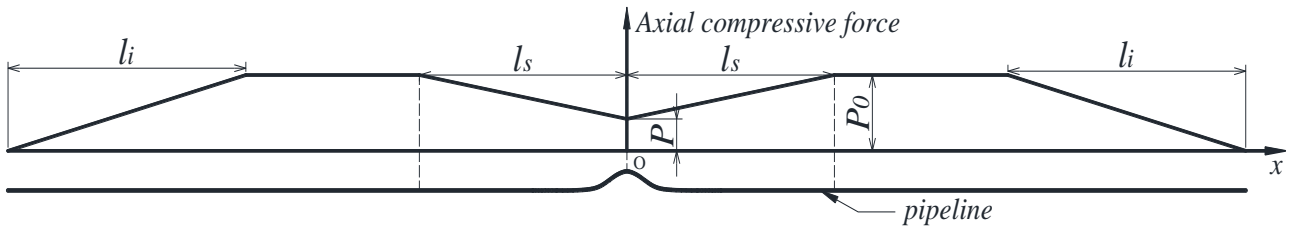Fig. 1 Configuration and load distribution of localised upheaval buckling.

Fig. 2 Axial compressive force distribution of localised upheaval buckling.

2.1 Pipeline buckling under thermal loads

We imagine a pipeline buried in the seabed and subjected to a temperature difference T_0 between the fluid flowing inside the pipe and the environment. If the ends of the pipe are unrestrained then under an increase of the temperature difference the pipe will expand axially. This expansion will be resisted by friction between pipe and seabed (and surrounding soil). If the soil resistance for axial movement is constant, say f_A, then a compressive force will build up in the pipe, which will increase linearly with the distance from the freely-expanding end. At some point this compressive force is sufficient to halt further expansion of the central segment of the pipe. Thus an immobilised segment spreads from the centre of the pipe. The end points of this segment are called virtual anchor points. Between these points the compressive force in the pipe is equal to the force in a pipe with fixed ends under the same thermal load. Within the range of linear elastic response this compressive force can be written as

$$P_0 = EA\alpha T_0 \tag{1}$$

where E is the elastic modulus, A is the cross-sectional area of the pipeline and α is the coefficient of linear thermal expansion. Immobilisation will only occur if this compressive force is attained, which in the present scenario will only be the case if the length of the pipe is larger than $2l_i$, where

$$l_i = EA\alpha T_0/f_A \tag{2}$$

3

Under increasing temperature difference, the compressive force P_0 increases and at some point buckling may be initiated. As stated in the Introduction, for a sufficiently long pipe this will be localised buckling, with exponentially decaying deflection. For a pipe without imperfections we expect this buckling to occur in the centre of the pipe. Here we shall assume this buckling to be upheaval, i.e., vertical, against gravity and the resistance of the surrounding soil, rather than lateral. For a buried pipeline the lateral soil resistance is generally much larger than the vertical soil resistance, so upheaval buckling is normally dominant.

In the buckling process a small central segment of the pipe will mobilise. The same scenario as described above applies, but now in reverse. Thus, as pipe feeds into the buckle the compressive force in the pipe drops, pulling more pipe into the buckle. This feed-in will be halted at two more virtual anchor points at compressive force P_0 bounding the mobilised region. Fig. 2 shows the feed-in region within the larger immobilised pipe segment of length l_s with the localised buckle and the typical compressive force variation. l_s is sometimes called slip-length. In practice multiple (independent) localised buckles may form in the immobilised pipe segment, especially if it is long, but in the following we will present a theory for a single localised buckle.

2.2 Governing equations and boundary conditions

The buried pipeline subject to high temperature is idealised as an axial compressive Euler-Bernoulli beam supported by distributed springs on both sides in the vertical plane. The distributed springs simulate the nonlinear vertical soil resistance, which is provided by the soil foundation when the buried pipeline deforms vertically during the process of localised upheaval buckling. Fig. 1 illustrates the typical configuration of upheaval buckling for a buried subsea pipeline. Note that by symmetry we need only consider half the length of the pipe ($0 \leq x \leq l_s$). Thus we have the following equation for the vertical deformation of the pipeline

$$EI\frac{d^4w}{dx^4} + \bar{P}\frac{d^2w}{dx^2} + F = 0 \tag{3}$$

where w is the vertical displacement, EI is the bending stiffness, $\bar{P}$ is the axial compressive force and F is the nonlinear vertical soil resistance. We assume that $\bar{P}$ has the profile sketched in Fig. 2, i.e., $\bar{P} = P$ at the centre of the pipe and $\bar{P} = P_0$ at the end of the mobilised buckling region. Boundary conditions for Eq. (3), which must support localised solutions as in Fig. 1, will be discussed in detail in Section 2.4.

Axial deformation of the pipeline is governed by the equation

$$EA\frac{d^2u}{dx^2} = f_A \tag{4}$$

Eq. (4) is solved subject to the slip-length boundary conditions [10]

$$\begin{cases} u(l_s) = 0 \\ \frac{du}{dx}(l_s) = 0 \end{cases} \tag{5}$$

giving for the axial displacement

$$u(x) = \frac{f_A}{2EA}(x - l_s)^2 \tag{6}$$

We now use compatibility between axial and vertical deformation in the immobilised region $0 \leq x \leq l_s$ to derive a relationship between the axial compressive force P at the centre of the pipe and the temperature difference T_0. Compatibility can be expressed as

$$u_1 = u_2 \tag{7}$$

u_1 is the length of axial expansion within the pipeline section $0 < x < l_s$ due to high temperature. u_2 is the geometric shortening, which allows for the additional length introduced by the vertical displacement. Eq. (7) simply states that, since there are virtual anchor points at distance l_s from the centre of the pipe, the extra length of pipe in the buckle must come from axial expansion of the mobilised section of pipe.

We have

$$u_1 = \int_0^{l_s} \frac{\Delta\bar{P}(x)}{EA}dx \tag{8}$$

Here $\Delta\bar{P}(x)$ is the amount of decrease of axial compressive force along the pipeline after the pipeline buckles, given by

$$\Delta\bar{P}(x) = f_A(l_s - x) \tag{9}$$

Thus, we find

$$u_1 = \frac{f_A l_s^2}{2EA} \tag{10}$$

For u_2 we have

$$u_2 = \frac{1}{2}\int_0^{l_s}\left(\frac{dw}{dx}\right)^2 dx \tag{11}$$

Thus, combining Eq. (7) and Eq. (10), we obtain the following equation

$$l_s = \sqrt{\frac{2EAu_2}{f_A}} \tag{12}$$

By axial force balance, we have

$$P_0 - P = f_A l_s \tag{13}$$

Combining Eq. (1), Eq. (12) and Eq. (13), we finally obtain

$$T_0 = \frac{(P + \sqrt{2EAu_2f_A})}{EA\alpha} \tag{14}$$

For consistency we require l_s to be larger than the length of pipe in the localised buckle. Since there is no a priori guarantee that l_s as computed from Eq. (12) satisfies this condition, we need to check any computed solutions for acceptability.

2.3 Soil resistance

For the study of the influence of nonlinear vertical soil resistance on pipeline localised upheaval buckling, the selection of a suitable and practical vertical soil resistance model is of great importance.

2.3.1 Uplift peak resistance

The uplift peak resistance of a pipeline embedded in soil consists of four general components [42]: (1) submerged effective weight of the object; (2) submerged effective weight of the soil being lifted; (3) vertical component of the soil shearing resistance; and (4) vertical component of the suction force from excess pore pressure differences above and below the object.

The current prediction method for uplift peak resistance per unit length of the pipeline (R_{peak}) has evolved from the vertical slip-surface model developed by Schaminee et al. [43]. This assumes that the resistance to upheaval buckling is derived from both the weight of soil above the pipeline and from shear stresses on vertical shear planes originating from the sides of the pipe and propagating to the backfill soil surface. In cohesionless backfills, the assumption that the shear strength is directly proportional to the vertical effective stress implies that the uplift peak resistance (R_{peak}) can be expressed as

$$R_{\text{peak}} = \gamma'HD + \gamma'D^2\left(\frac{1}{2} - \frac{\pi}{8}\right) + f_p\gamma'\left(H + \frac{D}{2}\right)^2 + W_{\text{pipe}} \tag{15}$$

where $f_p = K\tan\phi$ is the uplift resistance factor, H is the cover depth from the ground surface to the top of the pipe, $\gamma' = 7840\,\text{N/m}^3$ is the submerged weight of the soil, K is the lateral earth pressure coefficient also accounting for increase in vertical stress during uplift, ϕ is the angle of internal friction, W_{pipe} is the submerged weight per unit length of the pipeline and D is the external diameter of the pipeline. This design equation is recommended in the design code DNV [1]. The friction coefficient corresponding to uplift peak resistance μ_{peak} can be expressed as

$$\mu_{\text{peak}} = R_{\text{peak}}/W_{\text{pipe}} \tag{16}$$

The key issue is to assess an adequate uplift coefficient f_p [1]. f_p can be calculated from a drained (peak) friction angle and a lateral earth pressure coefficient. It can also be calibrated from model test results. If the drained friction angle is known for the soil that is used in the model tests, then this can be used to calculate the lateral earth pressure coefficient K. For pipes in loose sand, test results indicate that an 'at rest' earth pressure model K_0 is appropriate for K, hence [1]

$$K_0 = 1 - \sin(\phi) \tag{17}$$

For pipes in medium sand and dense sand, a model K_p for K based on passive earth pressure theory provides the best fit to test data, hence [1]

$$K_p = \frac{1}{\left(\sqrt{1+\tan^2(\phi)}-\tan(\phi)\sqrt{1+r}\right)^2} \tag{18}$$

in which r is a roughness parameter whose value is negative for the current application and possibly near -1. The results for the uplift resistance factor f_p are shown in Table 1. In this paper, the parameters for medium sand are used.

Table 1 Results for the uplift resistance factor f_p.

Sand type	ϕ (°)	K model	Roughness r	f_p
loose	30	K_0	N/A	0.29
medium	35	K_p	-1.00	0.47
dense	40	K_p	-0.97	0.62

2.3.2 Axial soil resistance

Current understanding of the mobilised soil loads on pipes due to axial pipe restraint (or differential axial displacement between soil and pipe) is mainly based on soil–pipe interface parameters and an assumed failure mechanism of the soil. The commonly used approach for the determination of axial loads on pipes buried in cohesionless soils is through the use of the simple formula [44]

$$f_A = \mu_{ps}\left(\gamma'\pi D\left(H+\frac{D}{2}\right)\left(\frac{1+K_0}{2}\right)+W_{pipe}\right) \tag{19}$$

The friction coefficient corresponding to the axial soil resistance is then

$$\mu_A = f_A/W_{pipe} \tag{20}$$

Here f_A is the axial soil load on the pipe (soil resistance) per unit length of the pipeline, K_0 is the coefficient of lateral earth pressure at rest for the soil, $\mu_{ps} = \tan(\delta)$ is the sliding coefficient of friction between the soil and pipeline and δ is the interface angle of friction between the soil and the pipeline. The value of μ_{ps} is 0.43 for a steel-coated pipe [4]. This formula is in wide use in the design of pipeline systems and has been recommended for the computation of axial soil loads by the ASCE [45] and by Honegger et al. [46].

2.3.3 The nonlinear vertical soil resistance model

The uplift soil resistance is nonlinear for the upward movement of pipeline. However, for the downward movement of pipeline, the downward vertical soil resistance increases rapidly to a very large value at a very small downward displacement, which is much larger than the uplift peak soil resistance. So we regard the foundation beneath the pipeline as rigid. We don't consider the influence of downward stiffness of vertical soil resistance. However, we consider the upward stiffness of vertical soil resistance. The nonlinear vertical soil resistance model, which is borrowed from a nonlinear lateral soil resistance model [47], is expressed by

$$\mu = \mu_{brk}\left(1 - e^{-a_1\left(\frac{w}{D}\right)^{a_2}}\right) + (\mu_{res} - \mu_{brk})\left(1 - e^{-a_3\left(\frac{w}{D}\right)^{a_4}}\right) \tag{21}$$

The vertical soil resistance can then be calculated by

$$F = \mu W_{pipe} \tag{22}$$

Here μ is the equivalent friction coefficient, μ_{brk} is the friction coefficient corresponding to the uplift peak resistance R_{peak}, μ_{res} is the friction coefficient corresponding to the residual resistance and a_i (i=1-4) are constant parameters. So the breakout resistance $F_{brk} = \mu_{brk}W_{pipe}$ and the residual resistance $F_{res} = \mu_{res}W_{pipe}$.

For upheaval buckling, the buried pipeline will lift off the seabed. So the residual resistance equals W_{pipe} and $\mu_{res} = 1$. The first term of Eq. (21) only accounts for the initial mobilisation of the uplift peak resistance R_{peak}, which is controlled by the coefficient a_1. The mobilisation distance of the uplift peak resistance is denoted by δ_f, as shown in Fig. 3. The second term of Eq. (21) provides a smooth exponential transition from the uplift peak resistance to the residual resistance, which is controlled by the coefficient a_3. The residual resistance here is the submerged weight of the pipeline. The values of

coefficients a_2 and a_4 remain essentially constant for all values of cover depth H and are assigned to be 1 for all cases. However, the value of a_3, which determines the distance required to mobilise the steady resistance, changes with cover depth H, as shown in Table 2. The uplift peak resistance calculated by Eq. (21) is a little smaller than the real uplift peak resistance R_{peak}. So we adjust the friction coefficient corresponding to the breakout resistance μ_{brk} to make the breakout resistance calculated by Eq. (21) equal to R_{peak}. The nonlinear vertical soil resistance model with different cover depths H is shown in Fig. 3. The parameters for different cover depth are shown in Table 2. The values of μ_{brk} and μ_A in Table 2 are calculated by Eq. (16) and Eq. (20), respectively. The values of μ_{brk} in Table 2 are chosen to make $R_{peak} = F_{brk}$. The values of a_1 and a_3 in Table 2 are selected to make the values of μ match the values of μ_{peak} for different cover depths H, as shown in Fig. 3.

Table 2 Parameters for different cover depths.

Cover depth H	μ_{peak}	μ_A	μ_{brk}	a_1	a_3
1D	2.86	1.67	3	200	2
2D	5.34	2.5	5.5	200	1.2
3D	8.63	3.33	8.8	200	0.8
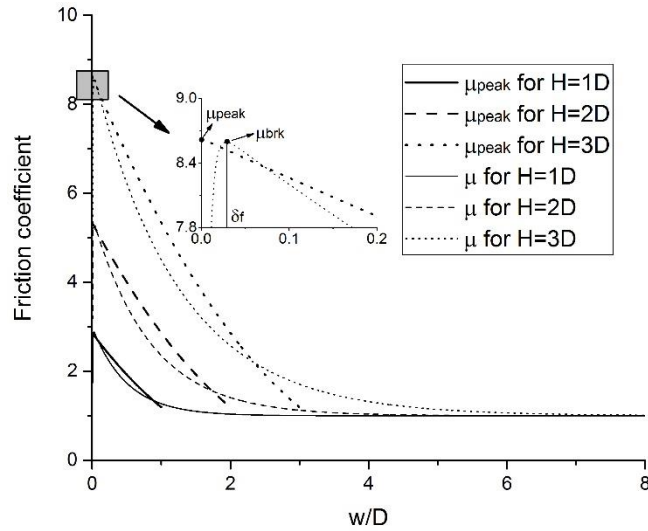
Fig. 3 Nonlinear vertical soil resistance model for different cover depth H.

2.4 Localised buckling

Here we discuss the localised solutions of Eq. (3). We now make the assumption that the axial compressive force is constant in the buckled region and equal to the force at the centre of the buckle, i.e., $\bar{P} = P$. The same approximation was made by Hobbs [9]. It is useful to rewrite the fourth-order Eq. (3) as an equivalent four-dimensional system of first-order equations $(w = w_1)$

$$\begin{cases} \dfrac{dw_1}{dx} = w_2 \\ \dfrac{dw_2}{dx} = w_3 \\ \dfrac{dw_3}{dx} = w_4 \\ \dfrac{dw_4}{dx} = -\dfrac{1}{EI}(Pw_3 + F) \end{cases} \tag{23}$$

Solutions of Eq. (23) are orbits in a four-dimensional phase space with coordinates (w_1, w_2, w_3, w_4). The straight pipe solution is represented by the fixed point j = (0, 0, 0, 0). The eigenvalues of the fixed point are

$$\pm i \sqrt{\frac{P \pm \sqrt{P^2 - 4EIk}}{2EI}} \tag{24}$$

where $k = \left(\frac{dF}{dw}\right)_{w=0}$. We conclude that at the critical load $P = P_{cr}$ with

$$P_{cr} = 2\sqrt{kEI} \tag{25}$$

the eigenvalues change from a quadruple of complex eigenvalues to two complex conjugate pairs of imaginary eigenvalues (see Fig. 4). This is called a Hamiltonian-Hopf bifurcation [37, 48] and marks the loss of stability of the straight solution. For comparison, the critical load for buckling of a pinned-pinned beam of n half sine waves is

$$P_{cr,periodic} = \frac{n^2 \pi^2 EI}{L^2} + \frac{kL^2}{n^2 \pi^2} \tag{26}$$

It is straightforward to show that $P_{cr} < P_{cr,periodic}$ for all n.

The symmetry and multiplicity of bifurcating solutions is governed by the symmetry of the system of equations. We have the following reversing symmetry (i.e., the equations are invariant under the following simultaneous sign changes)

$$R_1: \ x \to -x, \quad (w_1, w_2, w_3, w_4) \to (w_1, -w_2, w_3, -w_4) \tag{27}$$

It is well-known that among the solutions bifurcating from the trivial straight solution into the region of the complex quadruple of eigenvalues (here for $P < P_{cr}$) are so-called homoclinic orbits that leave the unstable fixed point in the plane spanned by the eigenvectors corresponding to the unstable eigenvalues (with positive real part), make a large excursion in the phase space and then return to the fixed point in the plane spanned by the eigenvectors corresponding to the stable eigenvalues (with negative real part) [48, 49]. These solutions thus approach the straight solution in both limits $x \to \pm\infty$ and are therefore also called localised solutions. Because of the above reversing symmetry, a symmetric (R_1-reversible) solution bifurcates. Half this localised solution is shown in Fig. 5-a, while the corresponding half orbit in (a two-dimensional projection of) the phase space is shown in Fig. 5-b. Note that the homoclinic orbits spiral out of (and back into) the fixed point because of the complex eigenvalues.

For later reference we also record here that for $P < P_{cr}$ the eigenvalues in Eq. (24) can be written as $\pm\lambda \pm i\omega$, with real λ and ω given by

$$\lambda = \frac{\sqrt{2\sqrt{EIk} - P}}{2\sqrt{EI}}, \qquad \omega = \frac{\sqrt{2\sqrt{EIk} + P}}{2\sqrt{EI}} \tag{28}$$

Expansion about the critical load gives

$$\lambda = \frac{\sqrt{P_{cr} - P}}{2\sqrt{EI}}, \qquad \omega = \sqrt[4]{\frac{k}{EI}} - \frac{P_{cr} - P}{4\sqrt{2EIP_{cr}}} + O((P_{cr} - P)^2) \tag{29}$$
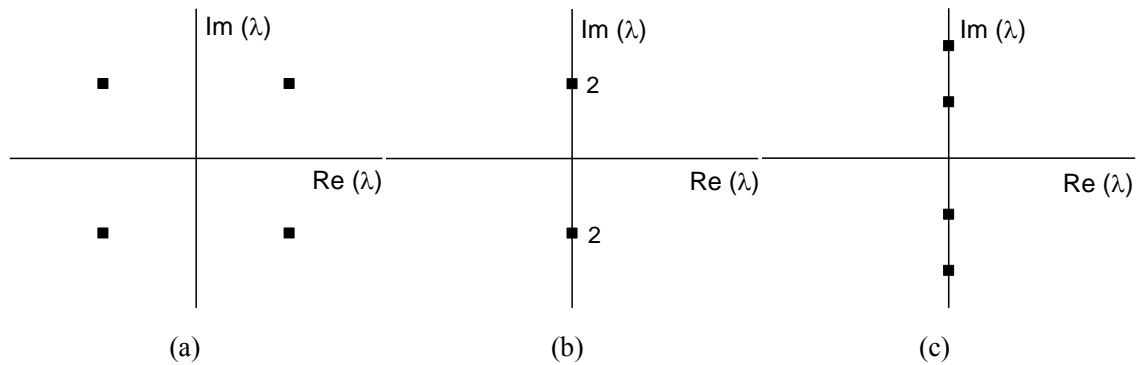

Fig. 4 The behaviour of eigenvalues at the Hamiltonian-Hopf bifurcation. (a) $P < P_{cr}$. (b) $P = P_{cr}$. (c) $P > P_{cr}$.
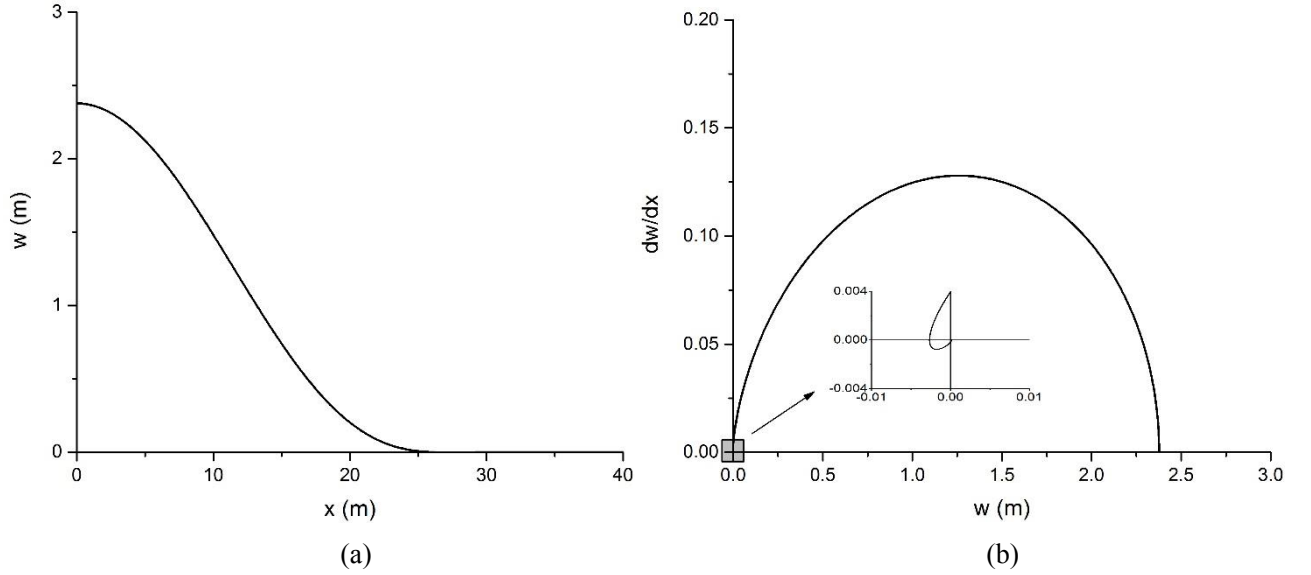
Fig. 5 Typical solution obtained by the shooting method. (a) Deformed shape. (b) Homoclinic orbit in phase space. $H = 2D$. $T_0 = 60\ ℃$.

3. Results

3.1 Numerical computation of localised solutions

For $P < P_{cr}$, we compute approximate (half) homoclinic solutions as in Fig. 5-a by formulating a shooting method on a truncated x interval $[-L, 0]$. Here L, the half length of the homoclinic solution, is chosen large enough that the solution is well-localised in the sense that it is very nearly decayed to the trivial straight solution j at $x = -L$. Thus we specify initial conditions

$$w(-L) = j + \varepsilon(v_1 \cos \delta + v_2 \sin \delta) \tag{30}$$

where $v_1 \pm iv_2$ are eigenvectors corresponding to eigenvalues $\lambda \pm i\omega$ of j. ε is a small constant, while δ and L are two shooting parameters that are initially guessed and iteratively updated by means of two boundary conditions. The parameter δ is the angle about the fixed point where the outward spiraling homoclinic orbit cuts the circle of radius ε around the fixed point in the unstable eigenspace. For the required two boundary conditions we take advantage of the symmetry properties in Eq. (27). We impose

$$\begin{cases} w_2(0) = 0 \\ w_4(0) = 0 \end{cases} \tag{31}$$

for symmetric solutions (see Fig. 5). The half orbits thus computed can readily be turned into full orbits by appropriate reflection according to R_1. Shooting over half the interval is numerically better behaved than shooting back into the neighbourhood of the unstable fixed point. The constant ε sets the scale of L. We choose $\varepsilon = 10^{-5}$, which is found to yield well-localised solutions.

The parameters used in this study are presented in Table 3. For these parameters and the additional choice $H = 2D$, we have $k = 3.2307 \times 10^6$ N/m. For the case $T_0 = 60\ ℃$, as shown in Fig. 5, the values of δ and L are 2.5215 and 47.7606 m, respectively. From Eq. (12) we also compute $l_s = 501.1783$ m, noting that this is larger than L, as required. The eigenvalues corresponding to the unstable manifold of the origin are $\lambda \pm i\omega$, where $\lambda = 0.3968$, $\omega = 0.4067$, and we use

$$v_1 = (0.8274, -0.3283, -0.0066, 0.1112)$$
$$v_2 = (0, 0.3365, -0.2670, 0.1033)$$

in Eq. (30).

Fig. 6 shows a bifurcation diagram obtained by varying the parameter P. w_m is the maximum vertical deflection. The plot in Fig. 6 confirms that the post-buckling localised solutions exist for loads smaller than the critical load P_{cr}, which, from Eq. (25), is $P_{cr} = 20.0202$ MN, i.e., the localised solutions bifurcate subcritically. Such subcritical bifurcations are well-

9

known to give rise to imperfection sensitivity [50]. Fig. 7 shows a solution for P =19.22 MN, close to the critical load, illustrating the oscillatory decay of the (small-amplitude) localised solutions governed by the eigenvalues $\pm\lambda\pm i\omega$. The wavelength of the solution, i.e., the distance between two successive maxima, is almost constant and agrees very well with the period $2\pi/\omega =11.3624$ m, while the decay rate $w_{m2}/w_{m1} =0.4637$ is well approximated by $e^{-2\pi\lambda} =0.4400$ (the agreement would be even better for values of P closer to P_{cr}). The asymptotic result in Eq. (29) shows that the decay rate depends on the distance from the critical load. The solution increasingly localises as the load P is reduced. For a (half) solution to be called localised the length L has to be larger than the localisation length L_l defined by

$$L_l = \frac{1}{\lambda} = 2\sqrt{EI/(P_{cr} - P)} \tag{32}$$

Typical loads P in pipelines stay well away from the critical load P_{cr}, and therefore in practice only a few oscillations (lobes) are visible and the solution is very well localised, as in Fig. 5-a. The fact that localisation is observed at values of P much lower than P_{cr}, where the straight pipe is stable, is usually explained by inevitable imperfections and dynamical disturbances. We also note that for the solution of Fig. 7, $l_s =2.3338$ m, which is much smaller than the length of rod in the localised buckle, so this solution does not satisfy the compatibility condition Eq. (7). All other solutions presented in this paper do satisfy this condition.

Table 3 Design parameters.

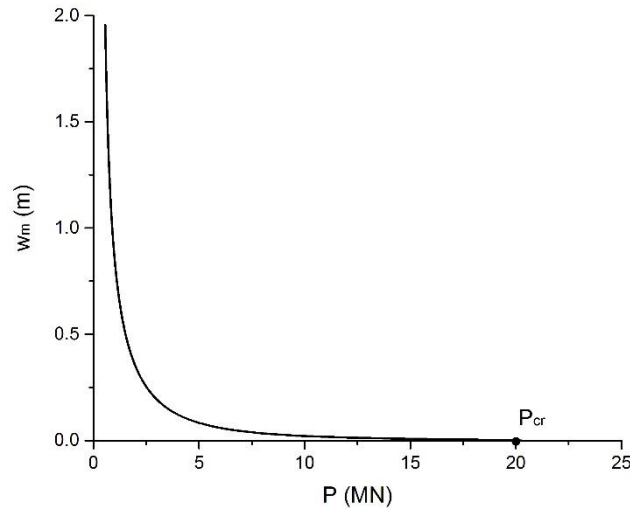| Parameters	Values	Unit
external diameter D	323.9	mm
wall thickness t	12.7	mm
elastic modulus E	206	GPa
coefficient of thermal expansion α	1.1×10^{-5}	/°C

Fig. 6 Bifurcation diagram with the branch of homoclinic orbits bifurcating subcritically at the critical load P_{cr}. $H = 2D$.
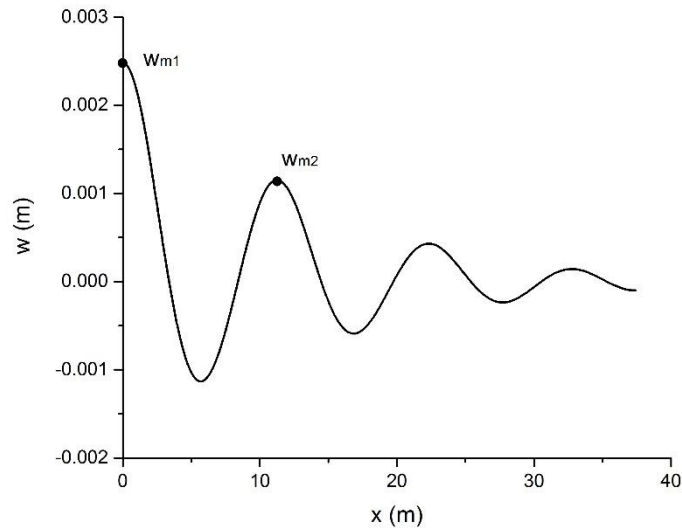
Fig. 7 The deformed shape close to the critical point. $P = 19.22$ MN. $H = 2D$.

3.2 Comparison with results in the literature

In this section, the localised upheaval buckling results of buried subsea pipelines with nonlinear soil resistance obtained by using the method described in the previous section are compared with the results of Hobbs [9]. In this case, the pipeline is unburied, so we take the uplift peak resistance R_{peak} equal to the pipe weight W_{pipe}. Also, the axial soil resistance is only induced by the pipe weight, so the friction coefficient corresponding to the axial soil resistance μ_A is taken equal to 0.43. The maximum vertical displacement w_m and maximum axial compressive stress σ_m for the unburied pipeline are shown in Fig. 8. We observe that the results from the present work are virtually identical to Hobbs's results.

The comparison between Hobbs's results and our analytical results for buried pipeline with cover depth $H = 2D$ is shown in Fig. 9. For Hobbs's results, the soil resistance is assumed to be equal to the uplift peak soil resistance, which is calculated by $\mu_{\text{peak}} W_{\text{pipe}}$. For our analytical results, a nonlinear soil resistance model is used. It is clear in Fig. 9 that the prediction of the critical temperature difference T_m by Hobbs is much larger than that with the nonlinear soil resistance model. Under the same temperature difference, the maximum vertical displacement w_m is smaller and the maximum axial compressive stress σ_m is larger for Hobbs's prediction. So we conclude that the nonlinear soil resistance must be taken into consideration for buried pipelines in the analysis of localised upheaval buckling.

Our comparison shows that it is feasible and effective to obtain accurate results by using Hobbs's method on condition that the pipeline is unburied and the vertical resistance stays constant. However, Hobbs's method cannot be applied to localised upheaval buckling when the vertical soil resistance is nonlinear as is the case for buried subsea pipelines. Moreover, the design formula in DNV-RP-F110 does not take the force-displacement curve for vertical soil resistance into account [1]. So it is necessary to study the effect of nonlinear vertical resistance on localised upheaval buckling.
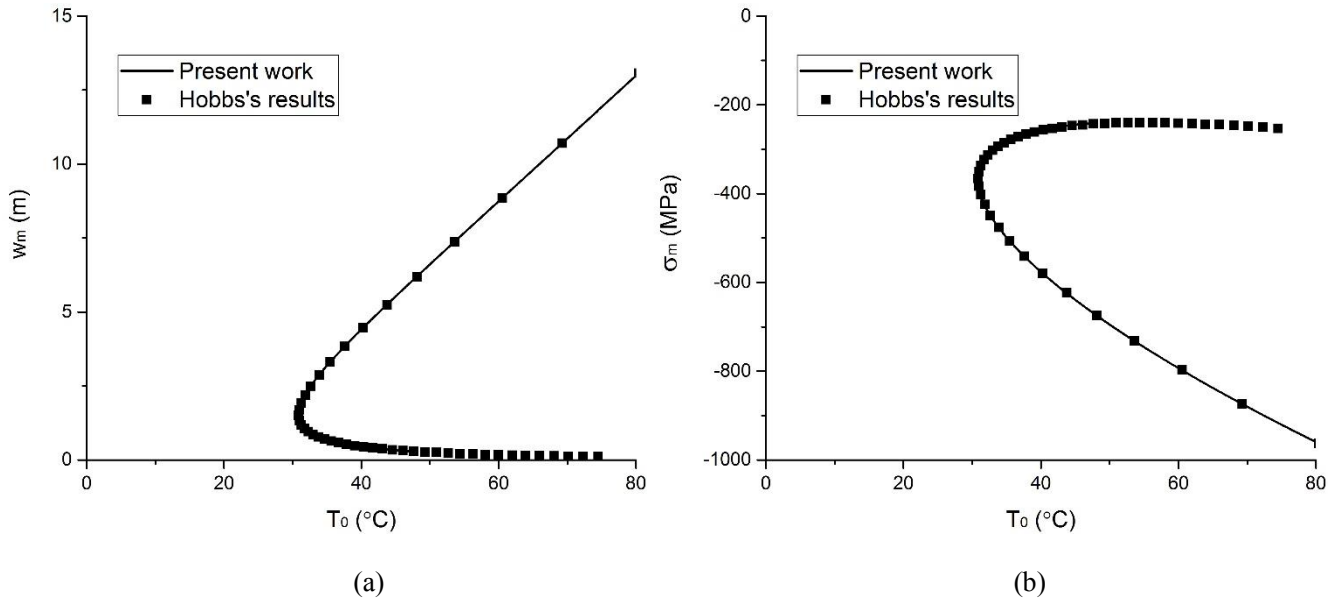
(a)   (b)

Fig. 8 Comparison of buckling paths with Hobbs's solutions. (a) Maximum vertical displacement w_m. (b) Maximum axial compressive stress σ_m. $\mu_{peak} = 1$, $\mu_A = 0.43$.
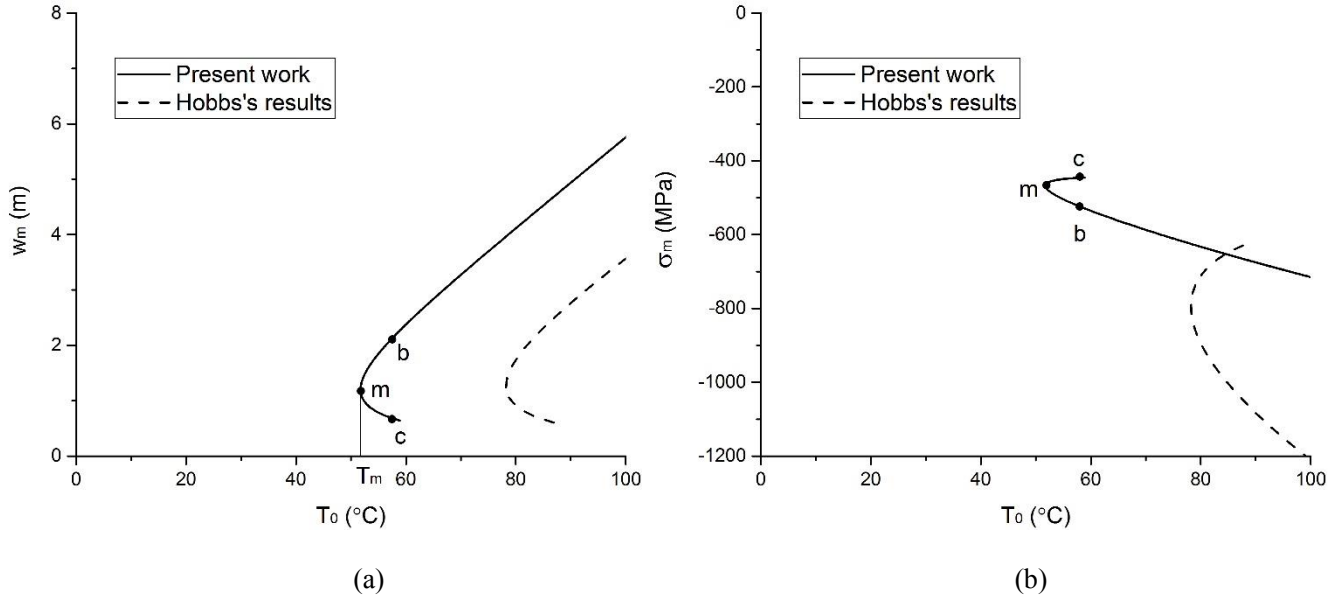

(a)   (b)

Fig. 9 Comparison of buckling paths with Hobbs's solutions. (a) Maximum vertical displacement w_m. (b) Maximum axial compressive stress σ_m. Cover depth $H = 2D$. $\mu_{peak} = 5.34$, $\mu_A = 2.5$.

3.3 The influence of the vertical soil resistance model

In this section, the influence of the vertical soil resistance model on localised upheaval buckling behaviour is presented and analysed by varying the values of the coefficients a_1 and a_3 that control the mobilisation distance of the uplift peak resistance δ_f and the rate of decay from the uplift peak resistance to the residual resistance. The friction coefficient μ for different values of a_1 and a_3 in the nonlinear vertical soil resistance model as well as the friction coefficient corresponding to uplift peak resistance μ_{peak} based on the cover depth $H = 2D$ are shown in Fig. 10. The corresponding parameters are listed in Table 4 and Table 5. We see in Fig. 10-a that the rate of decay from the uplift peak resistance to the residual resistance becomes faster with increasing a_3, while Fig. 10-b shows that the mobilisation distance δ_f increases with decreasing a_1.

Table 4 Parameters for different a_3. $H = 2D$.

a_3	μ_{peak}	μ_A	μ_{brk}	a_1
0.8	5.34	2.5	5.48	200
1.0	5.34	2.5	5.49	200
1.2	5.34	2.5	5.50	200
1.4	5.34	2.5	5.53	200

Table 5 Parameters for different a_1. $H = 2D$.

a_1	μ_{peak}	μ_A	μ_{brk}	a_3	δ_f
200	5.34	2.5	5.50	1.2	0.0082
100	5.34	2.5	5.62	1.2	0.0147
50	5.34	2.5	5.85	1.2	0.0260
25	5.34	2.5	6.30	1.2	0.0439

(a)	(b)
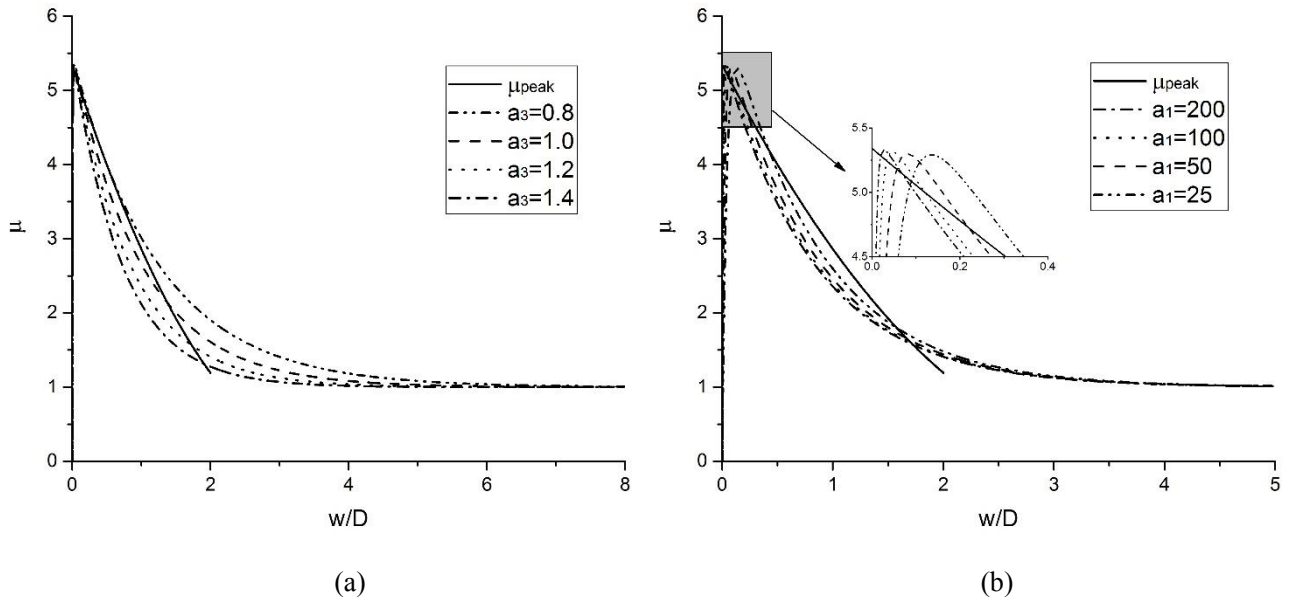
Fig. 10 Nonlinear vertical soil resistance model. (a) Different a_3. $a_1 = 200$. (b) Different a_1. $a_3 = 1.2$. $H = 2D$.

The deformed shapes and the corresponding bending stresses $\sigma_M = EDw_3/2$ along the buckled pipeline with different a_3 under the same operating temperature difference T_0 are presented in Fig. 11. In Fig. 11-a, it is seen that a localised buckled shape is formed within a limited region in the middle of the pipeline due to the axial compressive force induced by the temperature difference. This shape only consists of half a primary lobe in the positive direction ($w > 0$), while no other lobes exist in the negative direction ($w < 0$). This is different from lateral buckling because of large downward resistance. However, in some cases the seabed is soft enough to form another lobe in the negative direction ($w < 0$). For all values of a_3, the maximum vertical displacement occurs at $x = 0$ m and this maximum increases with increasing a_3, as shown in Fig. 11-a. However, the buckled region shrinks with increase of a_3. So we can conclude that the maximum vertical displacement is larger for faster rates of decay from the uplift peak resistance to the residual resistance. In Fig. 11-b, two maxima of bending stress (in absolute value) exist along the buckled region, with the maximum at $x = 0$ m larger than the other one. So the maximum bending stress occurs at $x = 0$ m and decreases slightly with increasing a_3. This means that the maximum bending stress is smaller for faster rates of decay from the uplift peak resistance to the residual resistance.
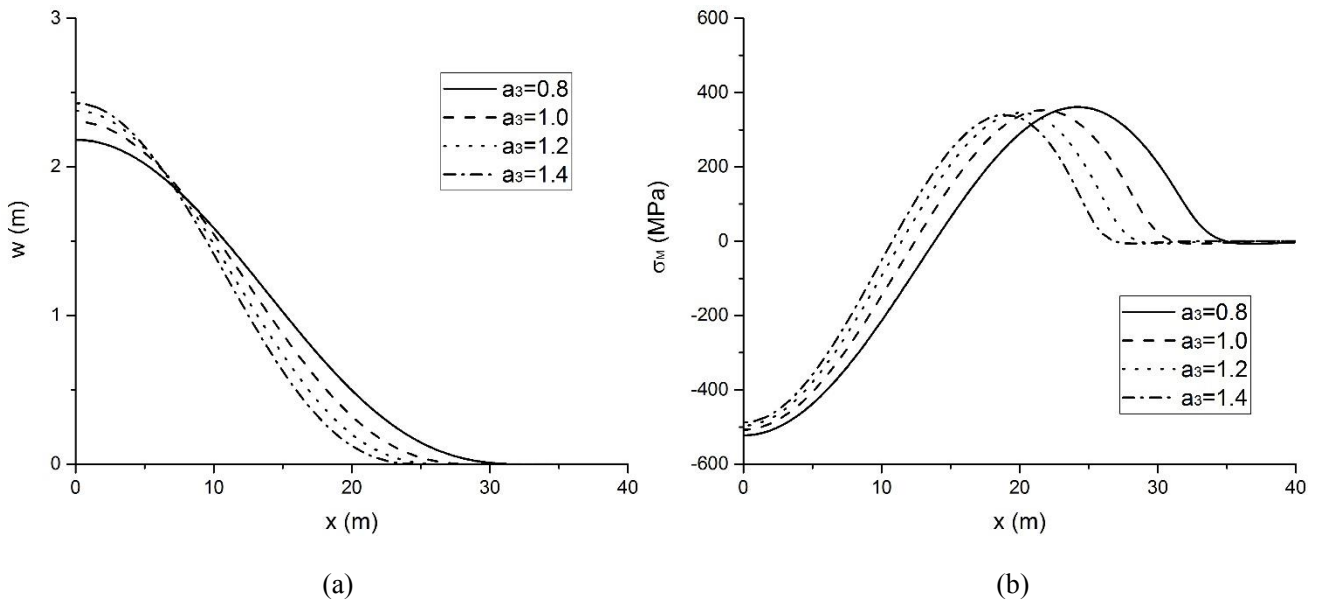
(a)

(b)

Fig. 11 The influence of a_3. (a) Deformed shapes. (b) Bending stresses. $T_0 = 60\ ℃$. $H = 2D$.
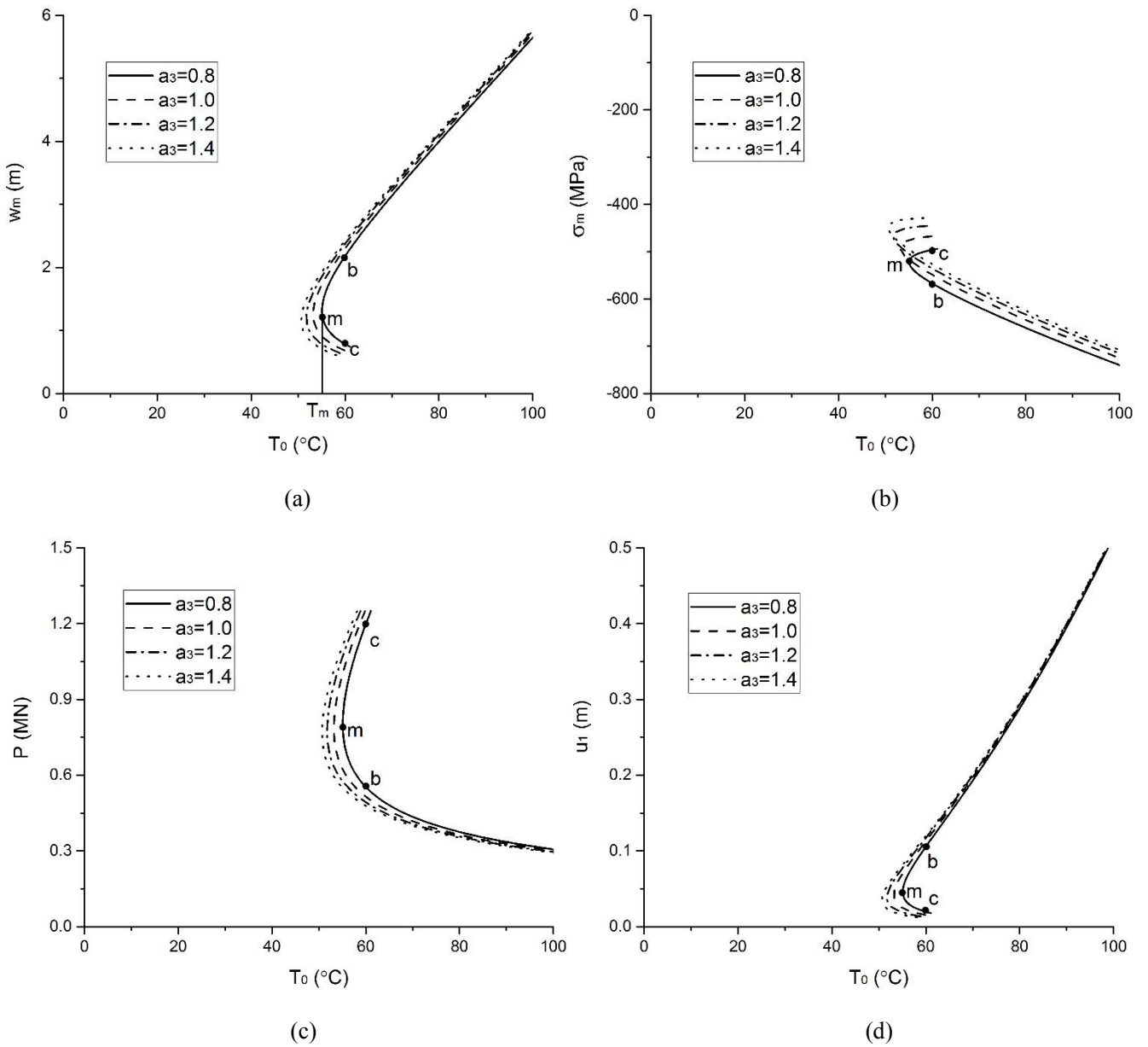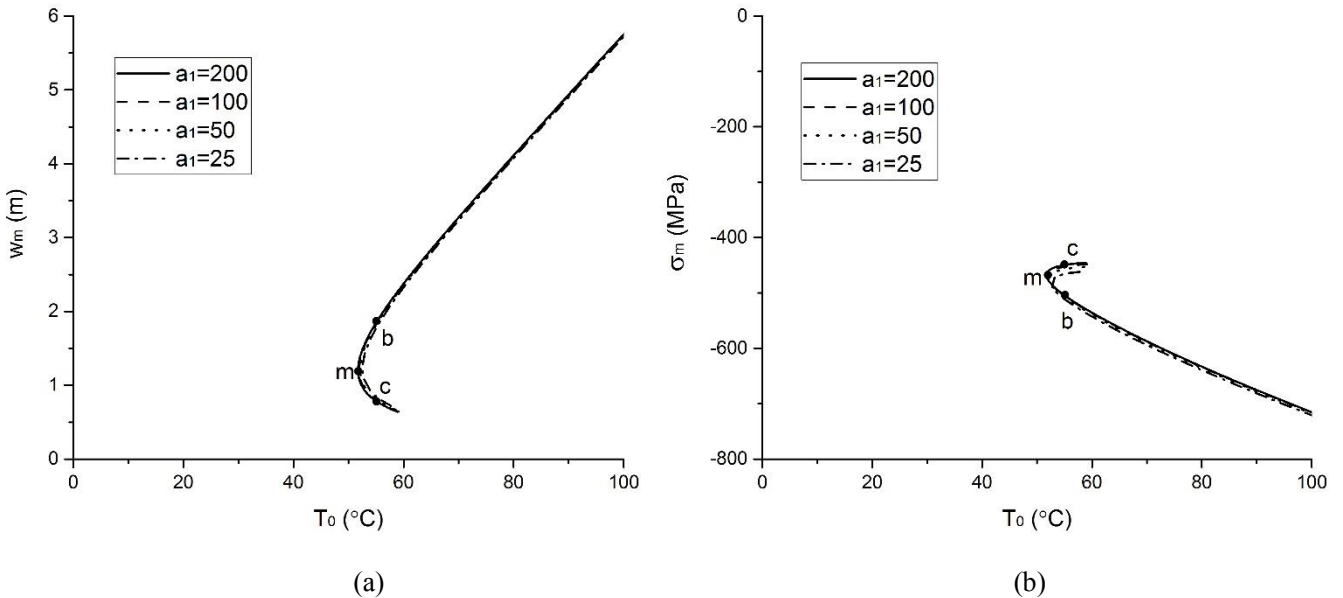

(a)

(b)

(c)

(d)

Fig. 12 The influence of a_3. (a) Maximum vertical displacement w_m. (b) Maximum axial compressive stress σ_m. (c) Axial compressive force P. (d) Axial thermal expansion u_1. $H = 2D$.

An energy analysis as in Wang and van der Heijden [39], which uses the deflection $w(x)$ as well as the axial displacement $u(x)$ computed in Eq. (6), shows that the branch m-b (see Fig. 12) is more stable than the trivial branch $w_m = 0$, in the sense that the localised solutions along branch m-b have lower total potential energy than the trivial straight-pipe solution at the same temperature difference T_0, while the branch m-c (see Fig. 12) is less stable than the trivial branch. So we expect to see solutions along branch m-b in practice and the following analysis is based on this stable branch m-b, as shown in Fig. 12.

The influence of a_3 on upheaval buckling behaviour is shown in Fig. 12. In Fig. 12-a, the minimum critical temperature difference T_m is seen to decrease with increasing a_3, which means that it will be easier for the pipeline to suffer upheaval buckling with faster rate of decay from the uplift peak resistance to the residual resistance. After upheaval buckling happens, the maximum vertical deflection w_m (see Fig. 12-a) and the maximum axial compressive stress σ_m (absolute value) (see Fig. 12-b) both increase with increasing temperature difference T_0. This is because the axial thermal expansion u_1 increases with increasing total temperature difference (see Fig. 12-d), which means that more u_1 will feed into the buckled region, leading to a more significant upheaval buckle. The maximum deflection w_m increases and the maximum axial compressive stress σ_m decreases with increasing a_3 under the same temperature difference T_0. The axial compressive force P decreases (see Fig. 12-c) and the axial thermal expansion u_1 increases (see Fig. 12-d) with increasing temperature difference T_0. Under the same temperature difference T_0, the axial compressive force P decreases and the axial thermal expansion u_1 increases with increasing a_3. Moreover, the difference of u_1 becomes smaller for increasing values of a_3 under the same temperature difference T_0. By contrast, the rate of increase of w_m and σ_m (absolute value) stays almost the same for increasing values of a_3. The reason for the difference between these different rates of increase is that the buckled region shrinks and the maximum deflection w_m increases with increasing a_3, as shown in Fig. 11-a.

The influence of a_1 on upheaval buckling behaviour is shown in Fig. 13. It is seen that the parameter a_1 has very little effect on the upheaval buckling behaviour, which means that upheaval buckling behaviour is barely affected by the mobilisation distance of the uplift peak resistance δ_f.
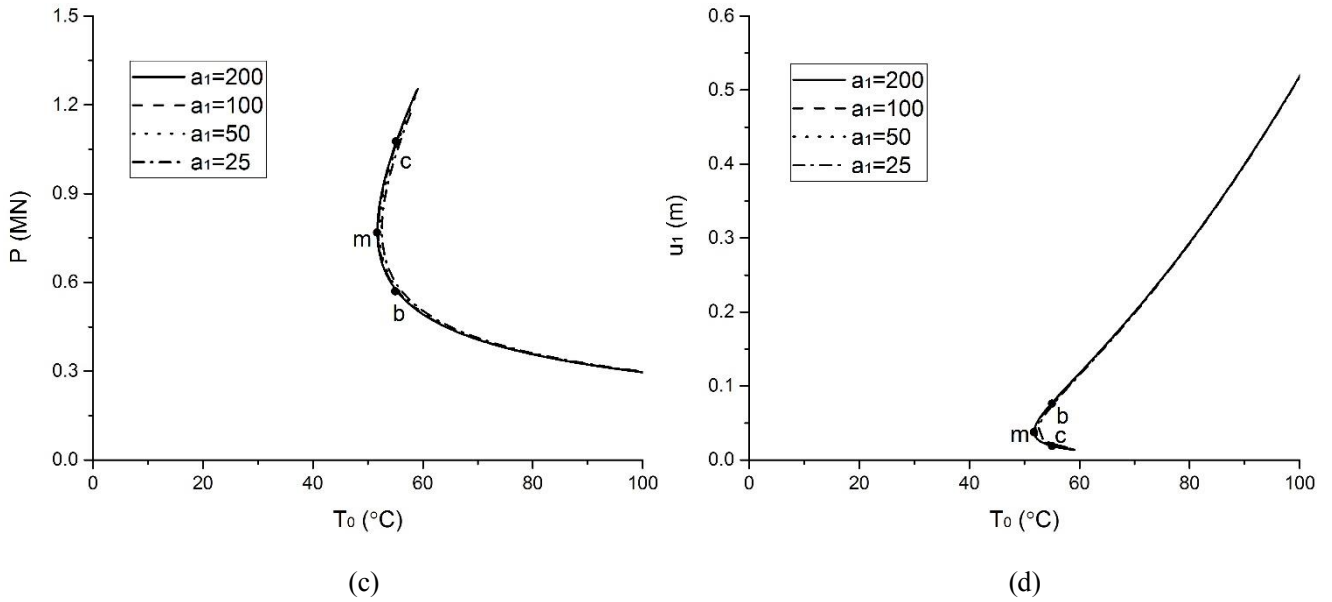

(a)

(b)

(c)

(d)

Fig. 13 The influence of a_1. (a) Maximum vertical displacement w_m. (b) Maximum axial compressive stress σ_m. (c) Axial compressive force P. (d) Axial thermal expansion u_1. $H = 2D$.

3.4 The influence of cover depth

In this section, the influence of the cover depth H on localised upheaval buckling behaviour is presented and analysed. The nonlinear vertical soil resistance models and the friction coefficient corresponding to uplift peak resistance μ_{peak} with different cover depths are shown in Fig. 3, while the corresponding parameters are listed in Table 2.

(a)

(b)
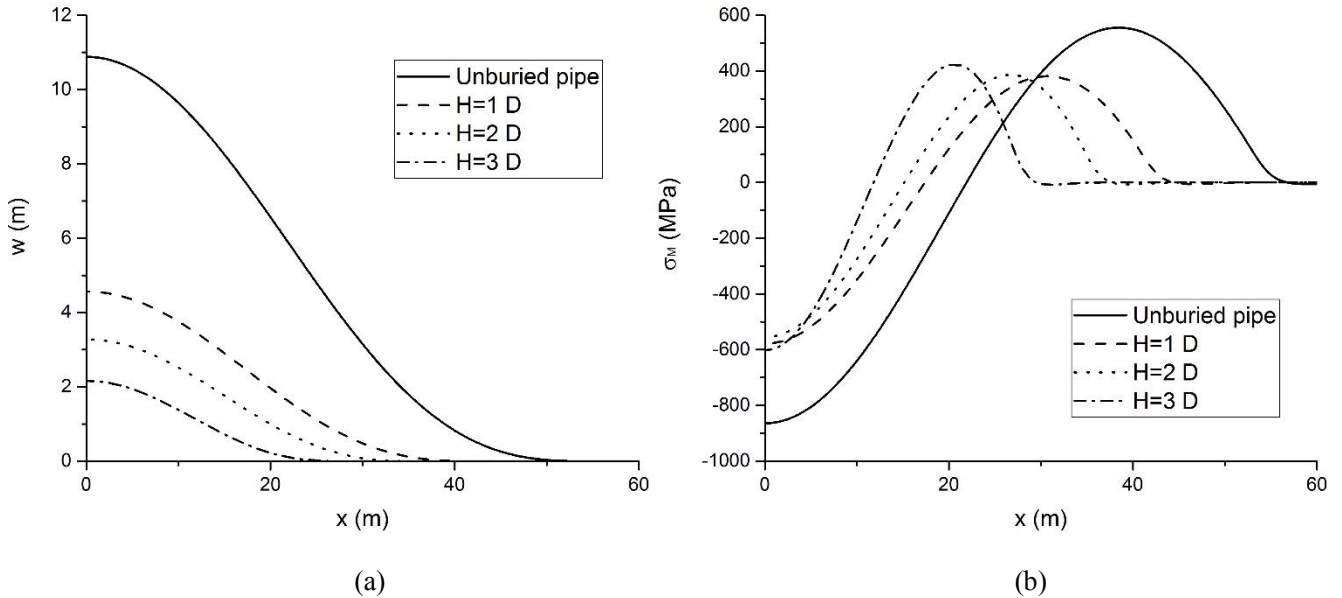
Fig. 14 The influence of cover depth H. (a) Deformed shapes. (b) Bending stresses. $T_0 = 70\ ^\circ\text{C}$.

The deformed shapes and the corresponding bending stresses $\sigma_M = EDw_3/2$ along the buckled pipeline with different cover depth H under the same operating temperature difference T_0 are presented in Fig. 14. In Fig. 14-a, it is seen that deformed shapes shrink with increasing cover depth H. Both the buckled region and the maximum vertical displacement decrease under increasing cover depth H. In Fig. 14-b we see two maxima of bending stress along the buckled region with the maximum bending stress occurring at $x = 0$ m. H does not have much influence on the bending stress maxima, except that for unburied pipeline the maximum stress is significantly larger. However, the location of the smaller maximum of bending stress moves to the central region with increasing cover depth H.

16

The influence of the cover depth H on localised upheaval buckling behaviour is shown in Fig. 15. In Fig. 15-a, the minimum critical temperature difference T_m is seen to increase with increasing H, which means that it will be more difficult for the pipeline to suffer upheaval buckling for larger H. This is the reason why pipelines are buried in an effort to prevent upheaval buckling. For buried pipelines, the rate of increase of the maximum deflection w_m stays almost the same under increasing cover depth, this maximum being smaller than that of the unburied pipeline, as shown in Fig. 15-a. The vertical deflection w_m decreases with increasing H under the same temperature difference T_0. The reason is that the axial thermal expansion u_1 decreases (see Fig. 15-d) with increasing H because of increasing axial soil resistance, resulting in less u_1 for larger H. However, there is not a regular pattern for the influence of H on the maximum axial compressive stress σ_m, as shown in Fig. 15-b, although we can conclude that the maximum axial compressive stress σ_m for a buried pipeline is smaller than that for an unburied pipeline under the same temperature difference T_0. From Fig. 15-c, the axial compressive force P increases with increasing H under the same temperature difference T_0.
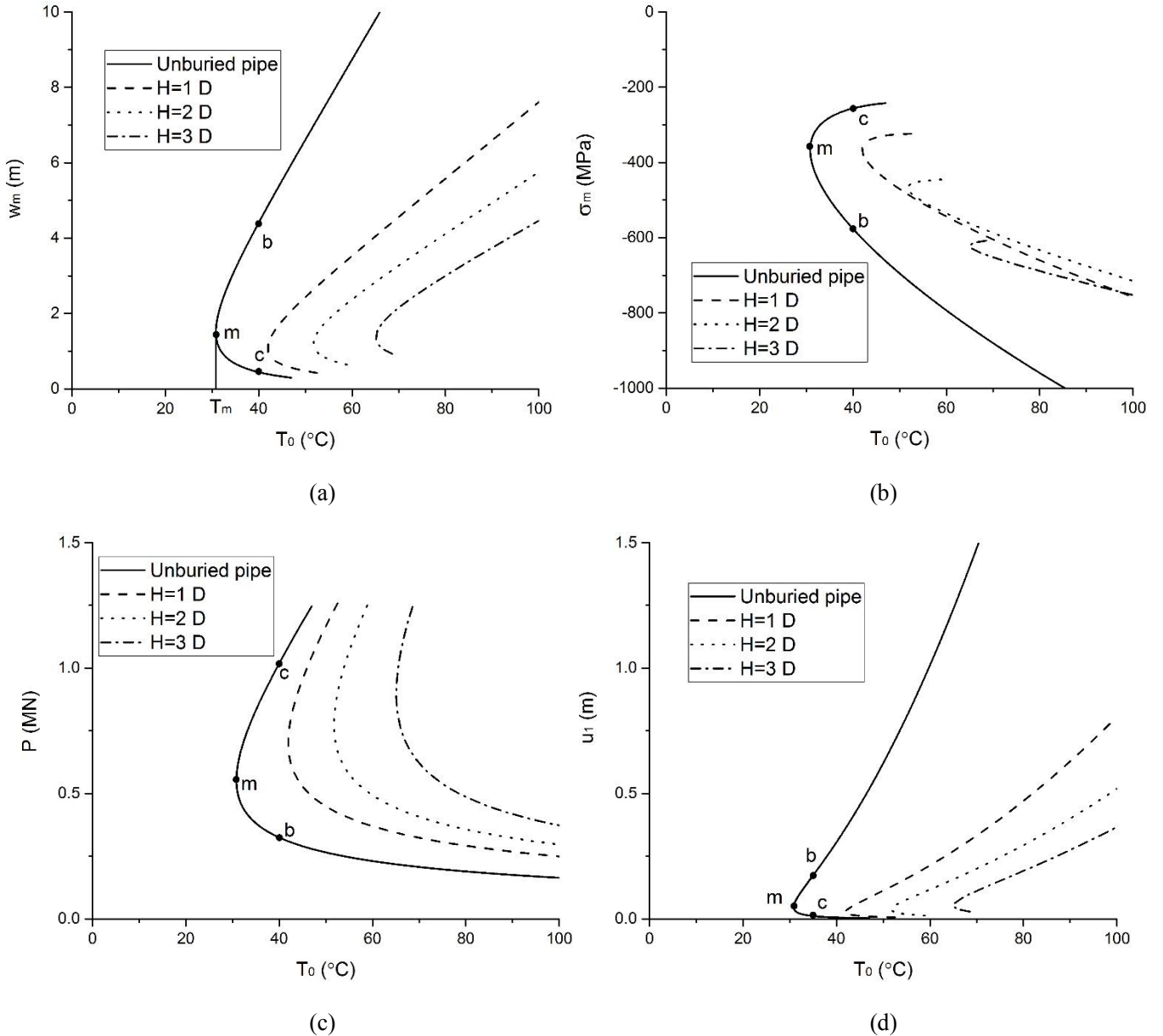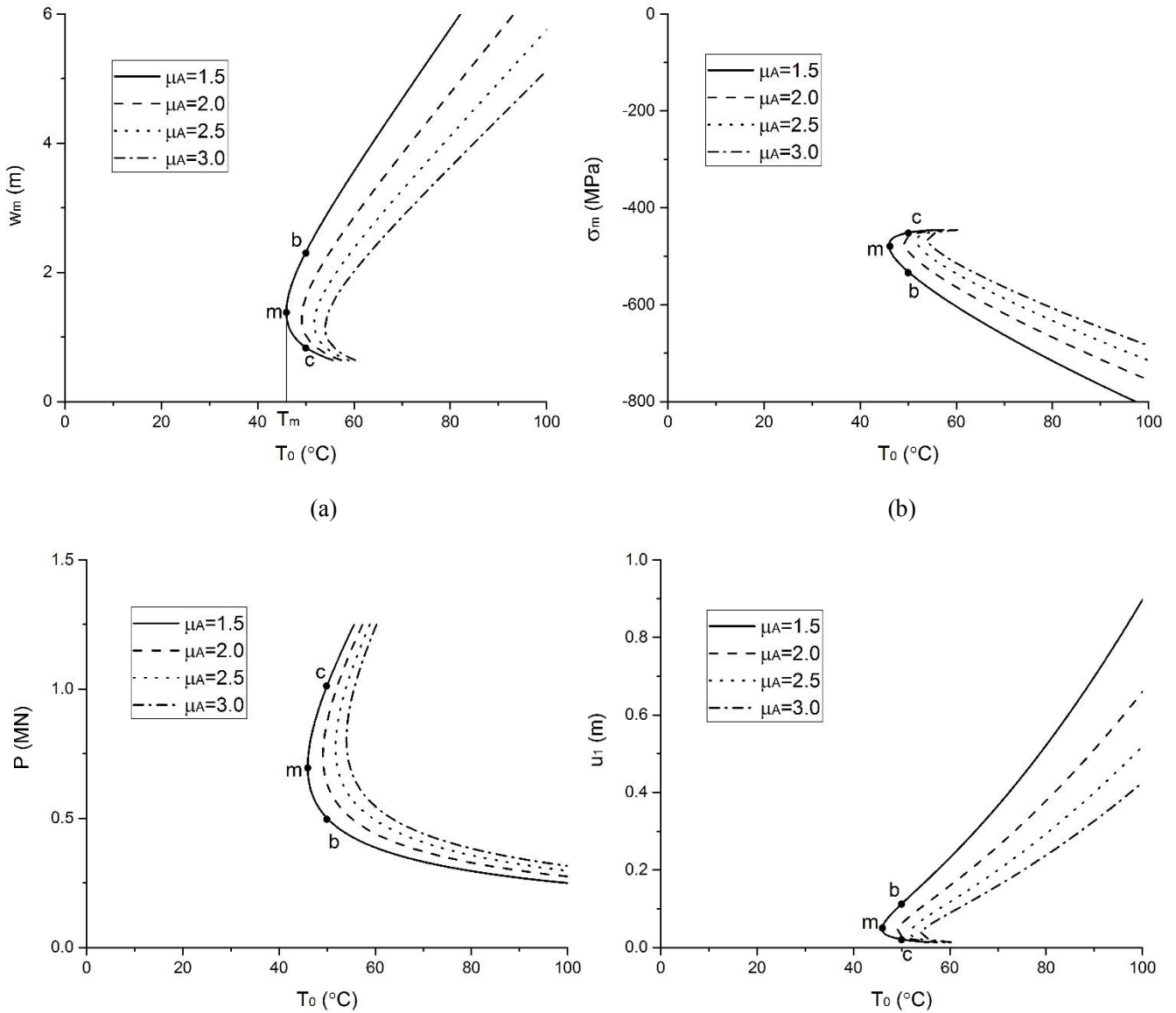

Fig. 15 The influence of cover depth H. (a) Maximum vertical displacement w_m. (b) Maximum axial compressive stress σ_m. (c) Axial compressive force P. (d) Axial thermal expansion u_1.

3.5 The influence of axial and uplift peak soil resistance

In the previous section, the influence of the cover depth H on localised upheaval buckling was analysed. We have seen that the uplift peak soil resistance increases with increasing H (Fig. 3), while μ_A also increases with increasing H (Table 2). However, the influence of H on the maximum axial compressive stress σ_m is complex. So in this section, the influence of axial soil resistance and uplift peak resistance on localised upheaval buckling behaviour is presented and discussed. The parameters for $H = 2D$ in Table 2 are employed in the nonlinear vertical soil resistance model.
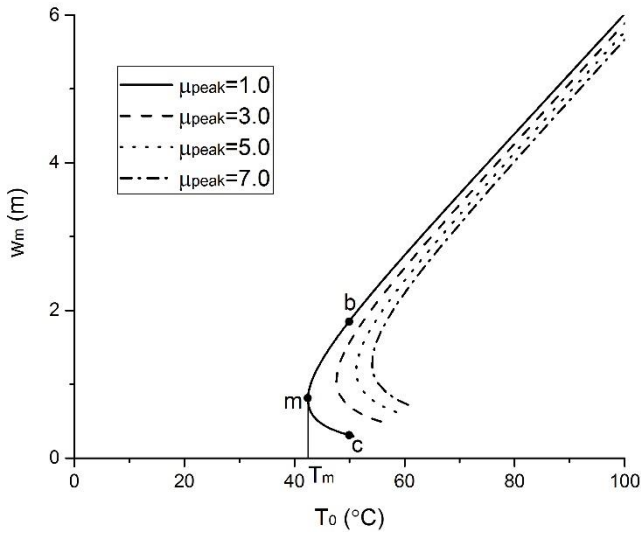
The influence of axial soil resistance and uplift peak soil resistance on localised upheaval buckling is presented in Fig. 16 and Fig. 17, respectively. The axial soil resistance and the uplift peak soil resistance are expressed by the corresponding friction coefficients μ_A and μ_{peak}, respectively. From Fig. 16-a and Fig. 17-a, the minimum critical temperature difference T_m increases with increasing μ_A and μ_{peak}. However, w_m decreases with increasing μ_A and μ_{peak} under the same temperature difference. The reason for this is that the axial thermal expansion u_1 decreases (see Fig. 16-d and Fig. 17-d) with increasing μ_A and μ_{peak} under the same temperature difference, resulting in less u_1 feeding into the buckle for larger μ_A and μ_{peak}. From Fig. 16-d and Fig. 17-d, the influence of μ_A on u_1 becomes larger while the influence of μ_{peak} on u_1 becomes smaller with increasing temperature difference, which leads to the same influence of μ_A and μ_{peak} on w_m (see Fig. 16-a and Fig. 17-a). From Fig. 16-b and Fig. 17-b, the maximum axial compressive stress σ_m decreases with increasing μ_A and increases with increasing μ_{peak} under the same temperature difference, which is the reason for the complex influence of H on σ_m, because both μ_A and μ_{peak} increase with increasing H. From Fig. 16-c and Fig. 17-c, we see that the axial compressive force P increases with increasing μ_A and μ_{peak} under the same temperature difference.
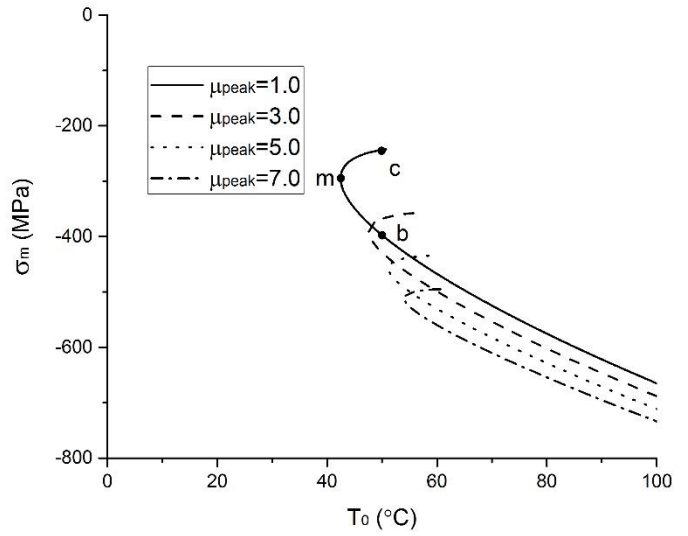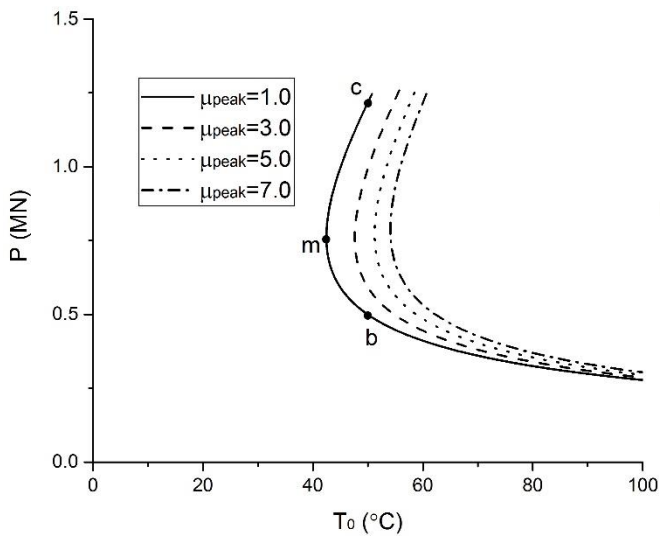

(a)

(b)

Fig. 16 The influence of axial soil resistance. (a) Maximum vertical displacement w_m. (b) Maximum axial compressive stress σ_m. (c) Axial compressive force P. (d) Axial thermal expansion u_1. $H = 2D$.
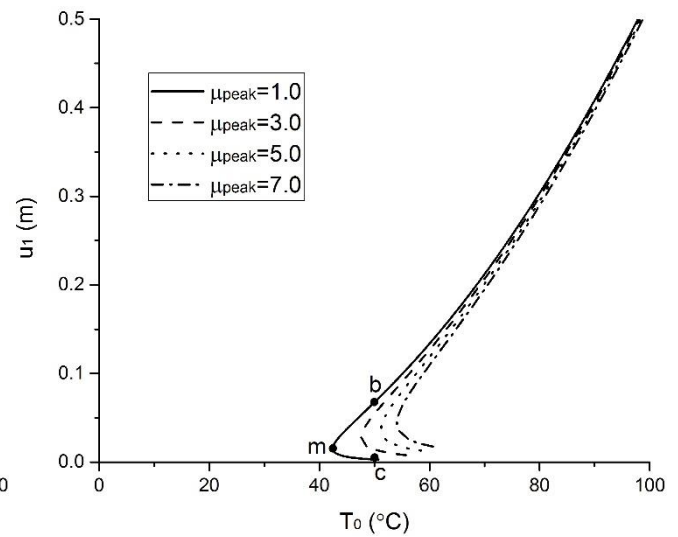

(a)

(b)

(c)

(d)

Fig. 17 The influence of uplift peak soil resistance. (a) Maximum vertical displacement w_m. (b) Maximum axial compressive stress σ_m. (c) Axial compressive force P. (d) Axial thermal expansion u_1. $H = 2D$.

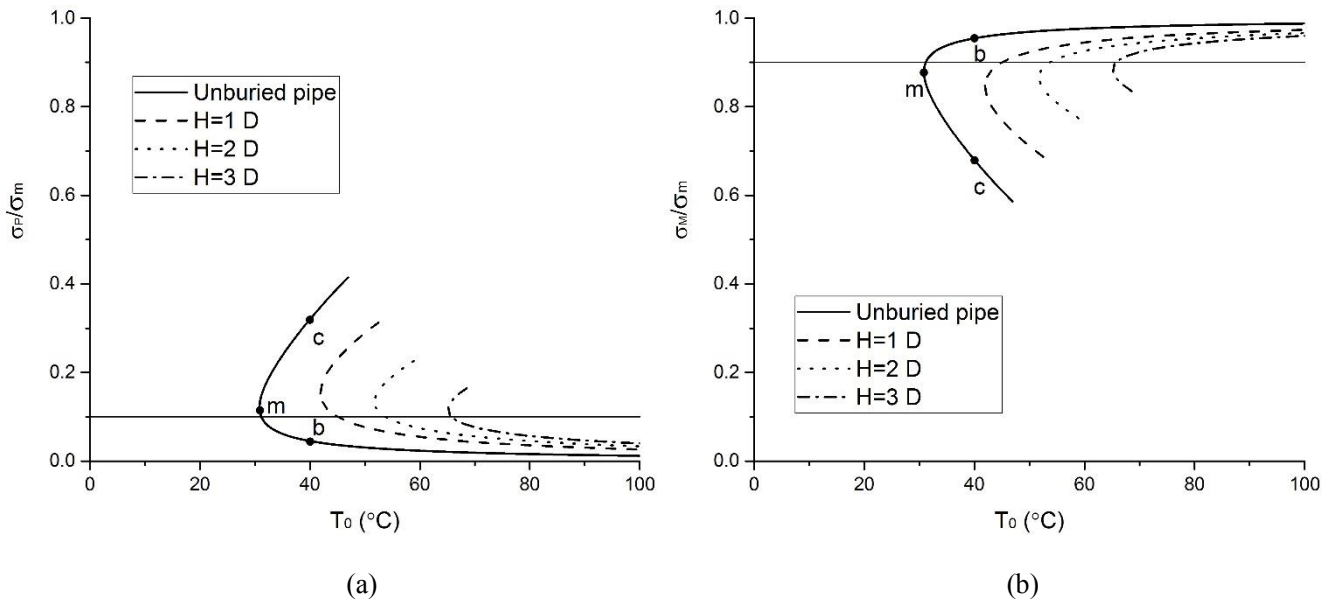## 3.6 The component of maximum axial compressive stress

(a)

(b)

Fig. 18 The influence of cover depth on the component of the maximum axial compressive stress σ_m. (a) σ_P/σ_m. (b) σ_M/σ_m.
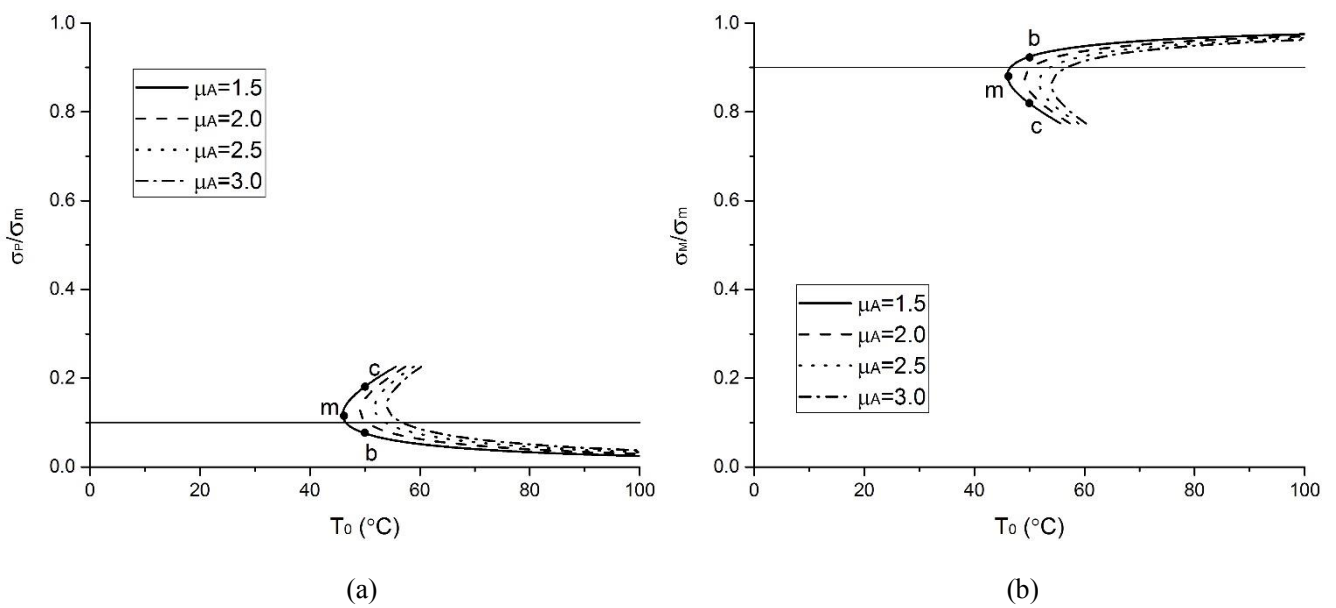

(a)

(b)

Fig. 19 The influence of axial soil resistance on the component of the maximum axial compressive stress σ_m. (a) σ_P/σ_m. (b) σ_M/σ_m. $H = 2D$.
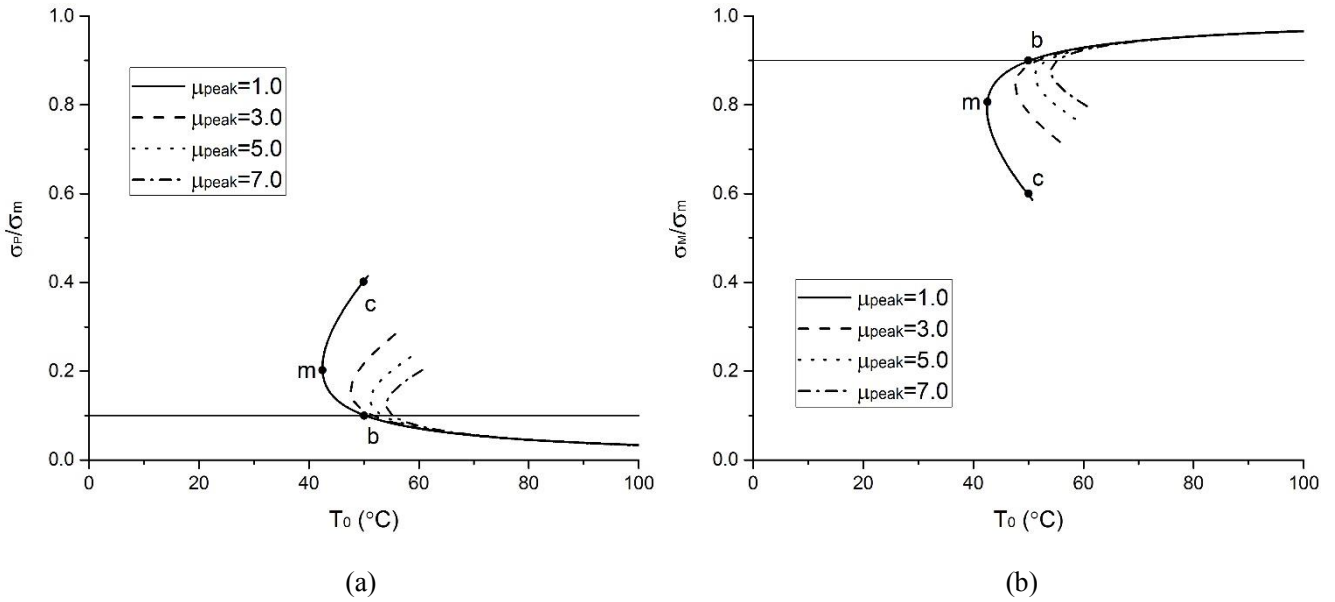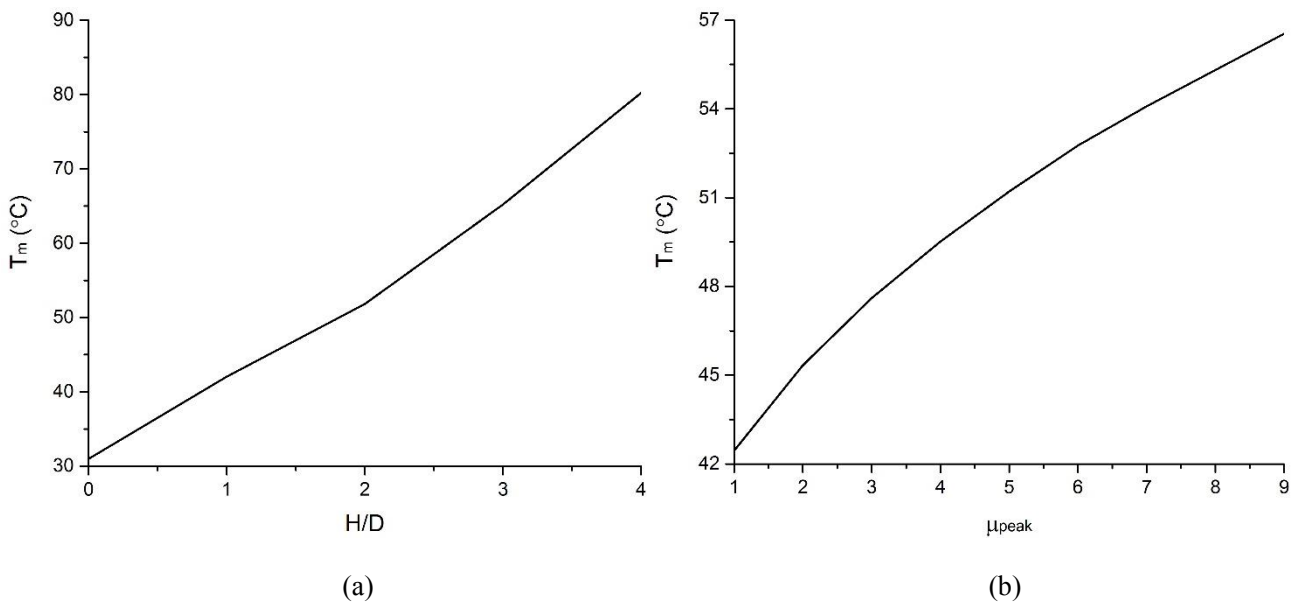
Fig. 20 The influence of uplift peak soil resistance on the component of the maximum axial compressive stress σ_m. (a) σ_P/σ_m. (b) σ_M/σ_m. $H = 2D$.

The influence of cover depth, axial soil resistance and uplift peak soil resistance on the component of the maximum axial compressive stress σ_m is shown in Fig. 18, Fig. 19 and Fig. 20, respectively. The maximum axial compressive stress σ_m consists of two parts, namely the bending stress σ_M induced by bending moment and the axial compressive stress $\sigma_P = P/A$ due to the post-buckling axial compressive force P. Branch m-b is relatively stable while branch m-c is relatively unstable [39], so only the stable branch m-b is analysed. For each specific case, σ_P/σ_m decreases and σ_M/σ_m increases with increasing temperature difference. From Fig. 18, σ_P/σ_m increases and σ_M/σ_m decreases with increasing H under the same temperature difference, which is induced by the increase of axial soil resistance because σ_P/σ_m increases and σ_M/σ_m decreases with increasing μ_A under the same temperature difference (see Fig. 19). However, μ_{peak} has little influence on σ_P/σ_m and σ_M/σ_m for larger temperature differences, as shown in Fig. 20. From Fig. 18, Fig. 19 and Fig. 20, over 90% of the maximum axial compressive stress σ_m is induced by the bending moment and less than 10% of the maximum axial compressive stress σ_m is induced by the post-buckling axial compressive force P in the post buckling stage. So the key point when trying to control the maximum axial compressive stress σ_m is to control the bending stress induced by the bending moment.
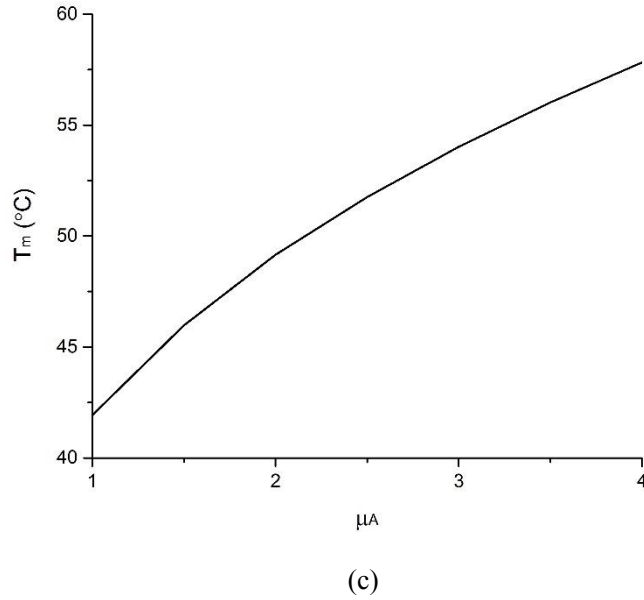
3.7 The minimum critical temperature difference

(a)

(b)

(c)

Fig. 21 Minimum critical temperature difference T_m. (a) Influence of H. (b) Influence of μ_{peak}. $H = 2D$. (c) Influence of μ_A. $H = 2D$.

The influence of the cover depth, axial soil resistance and uplift peak soil resistance on the minimum critical temperature difference T_m is illustrated in Fig. 21. The axial soil resistance and the uplift peak soil resistance are expressed by the corresponding friction coefficients μ_A and μ_{peak}, respectively, so the following analysis is based on μ_A and μ_{peak} using again the parameters for the case $H = 2D$. For the influence of μ_{peak} (Fig. 21-b) we take $\mu_A = 2.5$; for the influence of μ_A (Fig. 21-c) we take $\mu_{peak} = 5.34$. In Fig. 21 we see that the minimum critical temperature difference T_m increases with increasing H, μ_A and μ_{peak}. From Fig. 21-a, the minimum critical temperature difference T_m is 51.77 °C for $H = 2D$ and 65.21 °C for $H = 3D$. The increment in T_m is 13.44 °C when the cover depth H increases from $2D$ to $3D$. From Fig. 21-b, T_m is 51.77 °C for $\mu_{peak} = 5.34$, namely for $H = 2D$. When μ_{peak} increases to 8.63, namely for $H = 3D$, T_m increases to 56.09 °C, an increment in T_m of 4.32 °C. From Fig. 21-c, T_m is 51.77 °C for $\mu_A = 2.5$, namely for $H = 2D$. When μ_A increases to 3.33, namely for $H = 3D$, T_m increases to 55.33 °C, an increment in T_m of 3.56 °C. We conclude that the influence of separate increases in μ_{peak} and μ_A (see Fig. 21-b and Fig. 21-c) is smaller than that of a simultaneous increase in μ_{peak} and μ_A (see Fig. 21-a).

3.8 The effect of imperfection and internal pressure

The analysis so far has assumed that the profile of the pipeline is perfectly straight in the vertical plane, with no initial vertical offset. Three basic types of initial imperfection can be identified in practice. In the first case, the pipeline remains in continuous contact with some vertical undulation in an otherwise idealised horizontal and straight lay. The isolated prop alternatively features a sharp and distinct vertical irregularity such that voids (sea-filled) exist to either side. The third case occurs where the above voids become infilled with leaching sand and represents a special sub-case of the first [12]. The out-of-straightness or initial vertical imperfection can lower the safe temperature difference and affect the post-buckling behaviour. Therefore, it is important to investigate the effect of imperfections on the upheaval buckling of buried pipelines. In this analysis, a vertical deflection imperfection is imposed at the centre of the buckled section, the configuration of which is the configuration obtained in this paper. So only the magnitude of the initial imperfection w_{om} should be applied. There are two possible states for a initial imperfection: an unstressed pipe and a stressed pipe. The unstressed pipe corresponds to a local imperfection in the pipe itself, which means the initial state of the pipeline with such an imperfection is unstressed. The stressed pipe represents the case where the unstressed pipeline is straight but where it forms an initial curvature due to the pipe-laying vessel's sway motion or foundation irregularities. So the imperfection included here is the stressed case. For this case, the equations governing the vertical deflection will not be affected. The effect of the initial imperfection is that an initial geometric shortening u_{20} exists. This shortening u_{20} can be calculated by Eq. (11) when the initial imperfection w_{om} is given. So, Eq. (14) should be rewritten as

22

$$T_0 = \frac{\left(P + \sqrt{2EAf_A(u_2 - u_{20})}\right)}{EA\alpha} \tag{33}$$
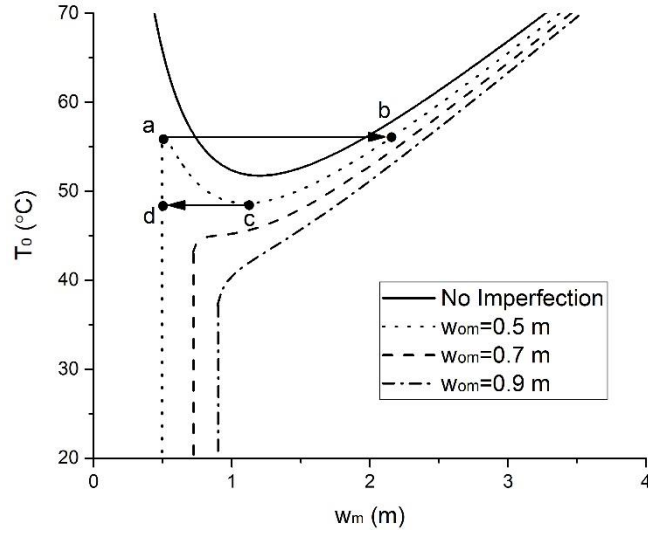

Fig. 22 The effect of imperfections on the load-deflection behaviour. Arrows indicate dynamic jumps under increasing (to the right) or decreasing (to the left) T_0. $H = 2D$.

The effect of imperfections on the load-deflection behaviour of the pipeline is illustrated in Fig. 22. We see that for smaller values of the imperfection, such as $w_{om} = 0.5$ m, the load-deflection curves have folds where dynamic jumps of the structure may occur under both increasing and decreasing temperature. Taking $w_{om} = 0.5$ m as an example, when the temperature difference increases to $T_0(a)$, the pipeline will jump from point a to point b if some disturbance occurs. With further increasing temperature difference, the pipeline will follow the post-buckling path. When the temperature difference decreases from $T_0(b)$ to $T_0(c)$, the pipeline will follow the post-buckling path from point b to point c. Then, the pipeline will jump from point c back to point d. For larger values of the imperfection, such as $w_{om} = 0.9$ m, the snap-through phenomenon disappears.

The effect of internal pressure for linear elastic material behaviour can be considered through the following formula [1, 9]

$$\Delta T_1 = \frac{pD(0.5 - v)}{2E\alpha t} \tag{34}$$

where p is the internal pressure of the pipeline, D is the pipe's external diameter, v is Poisson's ratio, generally equal to 0.3, α is the coefficient of linear thermal expansion and t is the thickness of the pipeline. The equivalent temperature difference ΔT_1 is generated by internal pressure.

4. Discussion and Conclusions

We have studied localised upheaval buckling of buried subsea pipeline by considering genuinely localised homoclinic solutions of the governing equations that bifurcate from a Hamiltonian-Hopf bifurcation. Our focus has been on the effect of the nonlinear pipe-soil interaction model on the load-deflection behaviour of the buckled buried subsea pipeline.

From our parameter studies the following conclusions can be drawn:

(i) At faster decay rates from the uplift peak resistance to the residual resistance, the buckled region shrinks, while the maximum vertical displacement increases and the maximum axial compressive stress decreases under the same temperature difference. The mobilisation distance of the uplift peak resistance has no appreciable effect on the upheaval buckling behaviour. So the decay rates from the uplift peak resistance to the residual resistance cannot be ignored. In future research, more attention should be paid to the decay rate from the uplift peak resistance to the residual resistance in the nonlinear vertical soil resistance model.

(ii) Under increasing cover depth, both the extent of the buckled region and the maximum vertical displacement decrease. However, the influence of cover depth on the maximum axial compressive stress is complicated with no regular pattern.

(iii) The maximum vertical displacement decreases with increasing axial and uplift peak soil resistance under the same temperature difference. The maximum axial compressive stress decreases with increasing axial soil resistance and increases with increasing uplift peak soil resistance under the same temperature difference, which is the reason for the complex influence of cover depth on the maximum axial compressive stress.

(iv) Over 90% of the maximum axial compressive stress is induced by the bending moment and less than 10% of the maximum axial compressive stress is induced by the post-buckling axial compressive force in the post-buckling stage.

(v) The minimum critical temperature difference decreases with increasing rate of decay from the uplift peak resistance to the residual resistance, which however increases with increasing cover depth, axial and uplift peak soil resistance. Moreover, the influence of separate increase in uplift peak soil resistance and axial soil resistance is smaller than that for the simultaneous increase in uplift peak soil resistance and axial soil resistance, which means that simple superposition is invalid for the influence of uplift peak soil resistance and axial soil resistance.

(vi) For relatively small values of the imperfection, a snap-through instability occurs, which disappears for sufficiently large imperfections.

Acknowledgments

References

[1] DNV-RP-F110. Global buckling of submarine pipelines structural design due to high temperature/high pressure. Det Norske Veritas; 2017.

[2] Cheuk CY, Take WA, Bolton MD, Oliveira J. Soil restraint on buckling oil and gas pipelines buried in lumpy clay fill. Engineering Structures. 2007;29:973-82.

[3] Bruton D, White DJ, Cheuk CY, Bolton MD, Carr M. Pipe-soil interaction behavior during lateral buckling, including large-amplitude cyclic displacement tests by the SAFEBUCK JIP (OTC-17944-MS). Offshore Technology Conference 2006. p. 1-10.

[4] Wang Z, Tang Y, Feng H, Zhao Z, Liu H. Model test for lateral soil resistance of partially embedded subsea pipelines on sand during large-amplitude lateral movement. J Coast Res. 2017;333:607-18.

[5] Wang J, Haigh SK, Forrest G, Thusyanthan NI. Mobilization Distance for Upheaval Buckling of Shallowly Buried Pipelines. J Pipel Syst Eng Pract. 2012;3:106-14.

[6] Brennan AJ, Ghahremani M, Brown MJ. Strength reduction for upheaval buckling of buried pipes in blocky clay backfill. Ocean Eng. 2017;130:210-7.

[7] Bransby MF, Ireland J. Rate effects during pipeline upheaval buckling in sand. Geotechnical Engineering. 2009;162:247-56.

[8] Hobbs RE. Pipeline buckling caused by axial loads. Journal of Constructional Steel Research. 1981;1:2-10.

[9] Hobbs RE. In-service buckling of heated pipelines. Journal of Transportation Engineering. 1984;110:175-89.

[10] Taylor N, Gan AB. Submarine pipeline buckling-imperfection studies. Thin-Walled Structures. 1986;4:295-323.

[11] Taylor N, Tran V. Experimental and theoretical studies in subsea pipeline buckling. Marine Structures. 1996;9:211-57.

[12] Taylor N, Tran V. Prop-imperfection subsea pipeline buckling. Marine Structures. 1993;6:325-58.

[13] Taylor N, Gan AB. Refined modelling for the vertical buckling of submarine pipelines. Journal of Constructional Steel Research. 1987;7:55-74.

[14] Taylor N, Gan AB. Refined modelling for the lateral buckling of submarine pipelines. Journal of Constructional Steel Research. 1986;6:143-62.

[15] Pedersen PT, Jensen JJ. Upheaval creep of buried heated pipelines with initial imperfections. Marine Structures. 1988;1:11-22.

[16] Croll JGA. A simplified model of upheaval thermal buckling of subsea pipelines. Thin-Walled Structures. 1997;29:59-78.

[17] Hunt GW, Blackmore A. Homoclinic and heteroclinic solutions of upheaval buckling. Proceedings of the Royal Society of London A: Mathematical, Physical & Engineering Sciences. 1997;355:2185-95.

[18] Maltby TC, Calladine CR. An investigation into upheaval buckling of buried pipelines-I. Experimental apparatus and some observations. International Journal of Mechanical Sciences. 1995;37:943-63.

[19] Maltby TC, Calladine CR. An investigation into upheaval buckling of buried pipelines-II. Theory and analysis of experimental observations. International Journal of Mechanical Sciences. 1995;37:965-83.

[20] Wang L, Shi R, Yuan F, Guo Z, Yu L. Global buckling of pipelines in the vertical plane with a soft seabed. Applied Ocean Research. 2011;33:130-6.

[21] Shi R, Wang L, Guo Z, Yuan F. Upheaval buckling of a pipeline with prop imperfection on a plastic soft seabed. Thin-Walled Structures. 2013;65:1-6.

[22] Hong Z, Liu R, Liu W, Yan S. Study on lateral buckling characteristics of a submarine pipeline with a single arch symmetric initial imperfection. Ocean Eng. 2015;108:21-32.

[23] Liu R, Liu W, Wu X, Yan S. Global lateral buckling analysis of idealized subsea pipelines. Journal of Central South University. 2014;21:416-27.

[24] Karampour H, Albermani F, Gross J. On lateral and upheaval buckling of subsea pipelines. Engineering Structures. 2013;52:317-30.

[25] Karampour H, Albermani F. Experimental and numerical investigations of buckle interaction in subsea pipelines. Engineering Structures. 2014;66:81-8.

[26] Karampour H, Albermani F, Veidt M. Buckle interaction in deep subsea pipelines. Thin-Walled Structures. 2013;72:113-20.

[27] Wang Z, Tang Y, Zhou L, Zhao Z, Wang C. Analytical solution for controlled lateral buckling of unburied subsea pipelines. Ocean Eng. 2017;146:140-50.

[28] Wang Z, Tang Y, Wang C. Analytical solution for lateral buckling of unburied subsea pipelines with distributed buoyancy section. Ocean Eng. 2017;146:115-24.

[29] Wang Z, Chen Z, Liu H, Bu Y. Static and dynamic analysis on upheaval buckling of unburied subsea pipelines. Ocean Eng. 2015;104:249-56.

[30] Wang Z, Chen Z, Liu H. Numerical study on upheaval buckling of pipe-in-pipe systems with full contact imperfections. Engineering Structures. 2015;99:264-71.

[31] Zhang X, Duan M. Prediction of the upheaval buckling critical force for imperfect submarine pipelines. Ocean Eng. 2015;109:330-43.

[32] Zeng X, Duan M, Che X. Critical upheaval buckling forces of imperfect pipelines. Applied Ocean Research. 2014;45:33-9.

[33] Xu L, Lin M. On the critical axial forces of upheaval buckling for imperfect submarine pipelines. Engineering Structures. 2017;147:692-704.

[34] Liu R, Basu P, Xiong H. Laboratory tests and thermal buckling analysis for pipes buried in Bohai soft clay. Marine Structures. 2015;43:44-60.

[35] Nazari A, Rajeev P, Sanjayan JG. Modelling of upheaval buckling of offshore pipeline buried in clay soil using genetic programming. Engineering Structures. 2015;101:306-17.

[36] Zhao T, Feng X. Upheaval buckling solution for submarine pipelines by segmented ditching and hot water flushing. Ocean Eng. 2015;102:129-35.

[37] Hunt GW, Bolt H, Thompson J. Structural localization phenomena and the dynamical phase-space analogy. Proceedings of the Royal Society of London A: Mathematical, Physical & Engineering Sciences. 1989;425:245-67.

[38] Zhu J, Attard MM, Kellermann DC. In-plane nonlinear localised lateral buckling of straight pipelines. Engineering Structures. 2015;103:37-52.

[39] Wang Z, van der Heijden GHM. Localised lateral buckling of partially embedded subsea pipelines with nonlinear soil resistance. Thin-Walled Structures. 2017;120:408-20.

[40] Zeng X, Duan M. Mode localization in lateral buckling of partially embedded submarine pipelines. International Journal of Solids and Structures. 2014;51:1991-9.

[41] Wang Y, Zhang X, Zhao Y, Chen H, Duan M, Estefen SF. Perturbation analysis for upheaval buckling of imperfect buried pipelines based on nonlinear pipe-soil interaction. Ocean Eng. 2017;132:92-100.

[42] Vesic AS. Breakout resistance of objects embedded in ocean bottom. ASCE Journal of the Soil Mechanics and Foundations Division. 1971;97:1183-205.

[43] Schaminee PEL, Zorn NF, Schotman GJM. Soil Response for Pipeline Upheaval Buckling Analyses: Full-Scale Laboratory Tests and Modelling (OTC-6486-MS).   Offshore Technology Conference1990. p. 1-10.

[44] Wijewickreme D, Karimian H, Honegger D. Response of buried steel pipelines subjected to relative axial soil movement. Canadian Geotechnical Journal. 2009;46:735-52.

[45] ASCE. Guidelines for the Seismic Design of Oil and Gas Pipeline Systems. New York: Committee on Gas and Liquid Fuel Lifelines, American Society of Civil Engineers   (ASCE); 1984.

[46] Honegger DG, Gailing RW, Nyman DJ. Guidelines for the Seismic Design and Assessment of Natural Gas and Liquid Hydrocarbon Pipelines (IPC2002-27330).   4th International Pipeline Conference2002. p. 563-70.

[47] Chatterjee S, White DJ, Randolph MF. Numerical simulations of pipe-soil interaction during large lateral movements on clay. Geotechnique. 2012;62:693-705.

[48] Van Der Heijden GHM, Champneys AR, Thompson JMT. The spatial complexity of localized buckling in rods with noncircular cross section. Siam Journal on Applied Mathematics. 1998;59:198-221.

[49] Champneys AR, Spence A. Hunting for homoclinic orbits in reversible systems: a shooting technique. Advances in Computational Mathematics. 1993;1:81-108.

[50] Hutchinson J, Koiter W. Postbuckling theory. Appl Mech Rev. 1970;23:1353-66.